Improved Steam Turbine Design for Optimum Efficiency and Reduced Cost of Ownership

Deshpande, Srikanth

2017

Document Version:
Publisher's PDF, also known as Version of record

Improved Steam Turbine Design for Optimum Efficiency and Reduced Cost of Ownership

Improved Steam Turbine Design for Optimum Efficiency and Reduced Cost of Ownership

by Srikanth Deshpande

LUND
UNIVERSITY

Thesis for the degree of Doctor of Philosophy
Thesis advisors: Assoc. Prof. Marcus Thern, Prof. Magnus Genrup,
Faculty opponent: Assoc. Prof. Lars O. Nord

To be presented, with the permission of the Faculty of Engineering of Lund University, for public criticism at the MA05 lecture hall (Matteannex) , LTH on Friday, the 5th of May 2017 at 10:00.

Organization
LUND UNIVERSITY

Division of Thermal Power Engineering
Department of Energy Sciences
Box 118
SE–221 00 LUND, Sweden

Document name
DOCTORAL DISSERTATION

Date of disputation
2017-05-05

Sponsoring organization

Author(s)
Srikanth Deshpande

Title and subtitle
Improved Steam Turbine Design for Optimum Efficiency and Reduced Cost of Ownership:

Abstract
The cost of ownership of a power plant is partly governed by the efficiency of the turbine island. The turbine stands for the production revenues when transforming the energy in fuel into electric power and district heating. One gauge of the quality of the individual processes is the component efficiency - the current work addresses the turbine part of the power plant. The turbine efficiency is dependent on both process parameters and the blading aerodynamics. The former is typically the steam data (e.g. temperature, pressure and mass flow) that influences the volumetric flow through the turbine. The blading aerodynamics is the local flow process in each stage in the turbine. The efficiency of a stage (i.e. a stator and a rotor) is limited by losses due to dissipation in boundary layers, losses due to secondary flows, leakage mixing and lost work, etc.

Most previous development efforts in the industrial steam turbine segment have been towards reduced first cost and not necessarily the efficiency. Most industrial steam turbines utilize prismatic (or un-twisted) blades for shorter stages. A constant section rotor blade typically is milled in a two-axis machine whilst more advanced shapes require five-axis flank milling. The costs associated with the latter have today leveled with the simpler manufacturing methods. This technology step has been introduced in larger size utility type of turbines with very high attainable efficiency levels. An industrial size steam turbine cannot reach the same level of efficiency and lags several points behind as for a utility type unit, because of the lower volumetric flow and the cylinder pressure ratio.

The focus in the present work has been to reduce the losses and hence increase efficiency in an industrial size steam turbine stage. Profile losses and secondary losses being the two main targets to improve performance, the work is focused on both the loss mechanisms.

The work has been carried out by state-of-the-art turbine design tools and comprises: one-dimensional tool, two-dimensional blade-to-blade flow analysis and full three-dimensional high-fidelity CFD. The datum stage is a tall stage in an assumed Siemens SST-900 turbine. The work, however, is generic for low-reaction steam turbines.

The work shows that the stage performance can be increased. The significant improvement obtained from numerical prediction makes a strong case for the proposed design modifications to be considered.

Key words
Steam Turbine, Aerodynamics, Flow Path Design, Efficiency, Coefficient of secondary kinetic energy (CSKE), Secondary kinetic energy helicity (SKEH)

Classification system and/or index terms (if any)

Supplementary bibliographical information

Language
English

ISSN and key title
0282-1990

ISBN
978-91-7753-227-9 (print)
978-91-7753-228-6 (pdf)

Recipient's notes

Number of pages
138

Price

Security classification

Signature _____ Date 2017-03-31

Improved Steam Turbine Design for Optimum Efficiency and Reduced Cost of Ownership

by Srikanth Deshpande

LUND
UNIVERSITY

Faculty of Engineering, Division of Thermal Power Engineering
Department of Energy Sciences

ISBN: 978-91-7753-227-9 (print)
ISBN: 978-91-7753-228-6 (pdf)
ISSN: 0282-1990

Printed in Sweden by Media-Tryck, Lund University, Lund 2017

Dedicated to my family

Contents

List of publications

I **Efficiency Improvements In An Industrial Steam Turbine Stage - Part 1**

Srikanth Deshpande, Marcus Thern, Magnus Genrup
ASME Turbo Expo 2016: Turbine Technical Conference and Exposition. American Society of Mechanical Engineers, 2016, Seoul, South Korea

II **Vortexing Methods to Reduce Secondary Losses in a Low Reaction Industrial Turbine**

Srikanth Deshpande, Marcus Thern, Magnus Genrup
ASME Turbo Expo 2015: Turbine Technical Conference and Exposition. American Society of Mechanical Engineers, 2015, Montreal, Canada

III **Influence of Compound Lean on an Industrial Steam Turbine Stage**

Srikanth Deshpande, Marcus Thern, Magnus Genrup
ASME 2015 Gas Turbine India Conference. American Society of Mechanical Engineers, 2015, Hyderabad, India

IV **Reduction in Secondary Losses in Turbine Cascade Using Contoured Boundary Layer Fence**

Srikanth Deshpande, Marcus Thern, Magnus Genrup
ASME 2014 Gas Turbine India Conference. American Society of Mechanical Engineers, 2014, New Delhi, India

V **Efficiency Improvements In An Industrial Steam Turbine Stage - Part 2**

Srikanth Deshpande, Marcus Thern, Magnus Genrup
ASME Turbo Expo 2016: Turbine Technical Conference and Exposition. American Society of Mechanical Engineers, 2016, Seoul, South Korea

VI **Effect Of Spanwise Variation of Chord On The Performance Of A Turbine Cascade**

Srikanth Deshpande, A.M.Pradeep, Marcus Thern, Magnus Genrup
To be presented at ASME Turbo Expo 2017: Turbine Technical Conference and Exposition. American Society of Mechanical Engineers, 2017, Charlotte, USA

Acknowledgements

A hundred times a day I remind myself that my inner and outer life depends on the labors of other men, living and dead, and that I must exert myself in order to give in the full measure I have received and am still receiving. - Albert Einstein

I would like to extend my sincere gratitude to my supervisors Prof. Magnus Genrup and Assoc. Prof. Marcus Thern for their support and guidance. I am grateful to Prof. Magnus Genrup for believing that I am good to pursue my doctoral studies at Lund University. The opportunity provided by him has brought in a complete shift in my life and has impacted my life in many good ways.

The research is funded by the Swedish Energy Agency and Siemens Industrial Turbomachinery AB through the Swedish research program KME at Energiforsk. The support is greatly acknowledged and appreciated. This funding has enabled us to explore, try, understand and most importantly contribute to the research topic. We thank Dr. Bertil Wahlund from Energiforsk for his support and guidance.

Sincere thanks to mentors and reviewers at Siemens Industrial Turbomachinery (SIT) in Finspång for their comments and feedback which has helped improve my understanding of turbine aerodynamics. Senior specialist, Lars Hedlund with his expertise in turbine aerodynamics and awareness of long history of steam turbines at SIT, helped us to understand key design philosophies. Åsa Nilsson and Dr. Markus Joecker, specialists at SIT supported greatly in building the baseline geometry and enabling the facilities required from SIT. Effort by Ken Flydalen, Manager of turbine aerodynamics to share his knowledge and understanding about airfoil design during a training session is greatly appreciated.

I thank Prof. Jens Klingmann for re-assuring my understanding on key fluid dynamics concepts and being open for very fundamental discussions about aerodynamics. Opportunity to teach alongside him was a great experience to cherish.

Being involved in design and numerical work, I was always curious to explore experimental turbine aerodynamics. An opportunity was provided in the form of funding by Erasmus ++ program. I could learn and conduct experiments at Turbomachinery Laboratory at Indian Institute of Technology, Bombay. I am grateful to Prof. Pradeep from Aerospace Engineering, Indian Institute of Technology, Bombay for providing the support. Also, sincere thanks to Prof. Magnus Genrup for giving me the freedom to step out and explore.

I thank my colleagues and friends at the division and department for their support and for creating encouraging atmosphere for research. Finally, I would like to thank my family here in Sweden as well as back in India for their unconditional support all the time.

Popular summary

The demand for energy and its resources is ever increasing globally. It is hence imperative to find efficient ways of producing energy. The better the efficiency of the comprising components in energy generation cycle is, the more will be energy produced for given resources and for lesser cost. Most energy generation cycles like the Rankine cycle, Brayton cycle and a few other recently developed cycles involve an important component, *turbine*. The turbine is the energy producing component in the cycle. Other key components in the cycle, like the compressor and the combustor assist the turbine to operate at very high efficiency and high power output.

The turbine section comprises of blade rows assembled axially. Each blade row may be a stator or a rotor depending upon the function. As the name indicates, a stator is a stationary blade row and a rotor is a rotating blade row. A stator row accelerates the flow and the rotor row converts the kinetic energy in the flow to mechanical energy. A combination of one stator row and one rotor row forms a *turbine stage*. There are many streams like mechanical design, aerodynamics design, manufacturing that collectively work for high performance of the turbine stage. The present work is an effort to improve the efficiency of a turbine stage from an aerodynamics perspective.

The turbine stage presented here is from a predefined stage in the (fictive) Siemens SST-900 turbine. SST-900 is an industrial steam turbine with a rating of approximately 200 MW which is owned by Siemens Industrial Turbomachinery AB, Finspång. This turbine has a long history and performs at good efficiency as it stands today. The task taken up in the present work is to further increase the aerodynamic efficiency of the turbine stage. Since the cross section of a blade row along the height of the blade is of airfoil section, the key things an aerodynamics design engineer needs to consider are : airfoil design, flow path design, how the airfoil sections are stacked along the height of the blade.

Increase in efficiency of a turbine blade row can be achieved by reducing the aerodynamic losses. Aerodynamic losses are predominantly of two kinds - profile losses and secondary losses. Profile losses originate from the design of airfoil sections and due to frictional losses due to wetted area. Profile losses cannot be completely eliminated but can be minimized. Secondary losses originate from the presence of the boundary layer along the blade height incident on the blade row. Efforts are made in the present work to minimize both profile losses and secondary losses. The loss mechanism that affects the performance of a blade depends vastly on the relative height of the blade when compared to its width. This relative geometric parameter is termed as aspect ratio. The higher the aspect ratio, more dominant will the profile losses be. Secondary losses are significant in low aspect ratio blades.

These efforts to reduce losses and increase efficiency can be experimental or numerical. The availability of resources, funds and timelines encourage the numerical analysis to be adopted

here to assess and improve aerodynamic efficiency. As a result of the present work, the understanding of the aerodynamic design of the existing turbine is enhanced. Also, an efficiency improvement of 0.74 % was achieved. The improvement was from reduction of profile losses.

Numerical analysis of the turbine stage with design modifications also revealed decrease in secondary losses. The parameter used to monitor secondary losses in numerical analysis is Secondary Kinetic Energy Helicity (SKEH). Hence, both profile loss and secondary loss reduction was aimed at in the present work.

Overall, the study presented has contributed to improve on the existing design with increased efficiency and better understanding of flow behavior in a turbine stage.

Nomenclature

c	blade chord
C_p	static pressure coefficient = $(P - P_1)/0.5\rho V_1^2$
P	pressure
h	total enthalpy
s	pitch - spacing between two adjacent blades
V	flow velocity

Greek letters

α	swirl angle
η	isentropic efficiency
ρ	local flow density, kg/m^3
ω	local flow vorticity

Subscripts

ax	axial direction
x,y,z	directional index
inlet	blade row inlet
exit	blade row exit
t	stagnation property
1	stage inlet
2	stator exit
3	stage exit / rotor exit
s	isentropic flow property

Acronyms & Abbreviations

CFD	Computational Fluid Dynamics
HP	High Pressure turbine section
IP	Intermediate Pressure turbine section
CSKE	Coefficient of Secondary Kinetic Energy
SKEH	Secondary Kinetic Energy Helicity
TPL	Total Pressure Loss

Introduction

Background

With the present global energy scenario, there is always a strive for increase in efficiency of contributing components in energy production. Turbine is one such component in the energy cycle which is looked at as an avenue to increase efficiency. Increase in efficiency directly results in reduced cost of ownership. To achieve efficiency increase in turbine from an aerodynamic perspective is the key objective of the work presented here.

With the target to increase the aerodynamic efficiency of a turbine, the study considering the whole turbine calls for huge resources. Hence, a single stage is considered for the study and attempts are made to increase the aerodynamic efficiency of the stage. It is assumed that the stage considered for efficiency improvement is representative of the turbine section.

The vehicle for the work presented is a predefined stage in (fictive but realistic) Siemens SST-900 turbine. SST-900 is an industrial steam turbine with a maximum rating of approximately 200 MW. The geometry and operational details of the stage to be considered for efficiency improvement was provided by industrial partners in the project, Siemens Industrial Turbomachinery AB, Finspång. The stage considered for study is from intermediate pressure section of SST-900. The design of this turbine section has a legacy with long history. With a long history, the efficiency of the turbine section already stands at considerably high numbers. To further improve upon the existing efficiency is a stiff challenge that is addressed in present study.

The stage considered for aerodynamic efficiency improvement comprises of prismatic blades. The flow path of the stage with the stator and rotor blades are shown in Fig.1. The word prismatic refers to constant airfoil section from root to tip i.e. constant spanwise metal angle. The objective of the present work is to improve on the aerodynamic efficiency when compared to the existing design. The motivation to increase the efficiency comes from the record efficiency numbers measured at Boxberg power plant [1]. Measured efficiency numbers of 94.2 % for high pressure section and 96.1 % for intermediate pressure section of steam turbine can be considered as landmarks in the performance history of turbines. Reports suggest that improvements in aerodynamic performance has contributed significantly

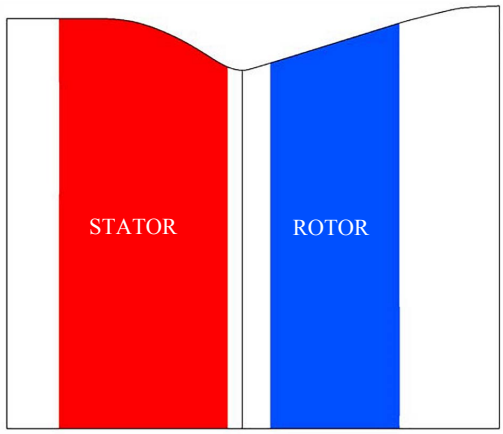

Figure 1: Stage from Intermediate pressure section of SST-900 .

for these high efficiency numbers.

Objectives

The overall research task is to improve the performance of an industrial size steam turbine, by introducing advanced blading technology. The basic parameters defining the stage are listed in Table.1. Reaction of the stage is low and also, blade row exit Mach numbers. Free stream Reynolds number being high is also a factor to be considered while modifying the airfoil design. Two prime loss mechanisms in turbomachinery flow being profile loss and secondary loss, focus is to reduce these to enhance performance. Better airfoil design is used to reduce profile losses whereas three-dimensional blading methods like vortexing and lean are predominantly used to reduce secondary losses. Vortexing methods are used to obtain required pressure distribution at blade row exit plane so that secondary flows and clearance flows can be minimized.

The objective is to improve performance of this stage. The function to quantify improvement in performance is primarily total to total efficiency. Total pressure loss is taken as a measure of bladerow performance for a stator or rotor. Along with this, coefficient of secondary kinetic energy and secondary kinetic energy helicity are used as functions to quantify and monitor secondary losses.

Table 1: Stage design parameters

Stage Loading Parameters	
Work coefficient	1.69
Flow coefficient	0.435
Degree of reaction	0.15

Blade Row Parameters		
Parameter	Stator	Rotor
Rel. exit Mach number	0.35	0.21
Exit Reynolds number	3.13×10^6	1×10^6
Pitch-to-chord ratio	0.78	0.71
Aspect ratio (axial chord)	2.1	3.13

Constraints

Design problems are typically imposed with constraints to work with. Constraints imposed to carry out the tasks in present work are three fold. The three non-dimensional parameters defining the turbine stage performance are to be maintained from the baseline case. i.e.

- Work coefficient: which defines the enthalpy drop in a turbine stage
- Flow coefficient: which defines the mass flow in a turbine stage
- Reaction: which restricts the area ratios in flow passage and in turn governs the axial thrust on rotor

With these constraints imposed, couple of things at disposal to work for performance improvement are, airfoil design and spanwise variation of flow parameters. Spanwise variation of flow parameters are typically attained by vortexing methods, lean, sweep and other three-dimensional blading methods.

The research field is related to turbine aerodynamics where the aim is to minimize the losses (i.e. entropy increase) in the turbine flow path. There are two ways to approach the research question, namely; numerically or experimentally. In this work, the former approach is adopted. The reason for not running experimental research is the prohibitive costs of a test turbine campaign and availability of such turbine.

The efficiency improvements in the considered stage is presented in the chapters in a way that the continuity is maintained for the reader. The chronological order of the papers presented are altered to facilitate a good read. Firstly, the numerical methodology adopted in design evaluation is presented. Chapters include reduction in profile losses to begin with.

Secondary loss reduction is discussed in subsequent chapter. Then, flow path modifications that were tried for better design of the stage are reported.

In addition to these chapters, a chapter on experimental study on a linear cascade that was performed as a part of the project is included. This study also supports the high pressure section of SST-900 wherein a specific distribution of chord is maintained in stator for ease of manufacturing. More details are provided in the corresponding chapter.

Numerical Methodology

Design modifications were analyzed numerically using commercial software CFX 15.0. Three-dimensional RANS simulations were carried out. Mixing plane approach with stage interface was used with specified pitch values. $k-\omega$ SST turbulence model was used and convergence criteria set was 1×10^{-5} for momentum and energy residuals. Transition model was not included in the analysis. Mass and energy imbalance was maintained below 0.001 % for all the runs. IAPWS steam tables were used to represent the fluid medium.

Domain Details

CFD context models for evaluating airfoil design modifications, vortex designs, lean implementations and flow path modifications were built using commercial software NX. This was used as interface between the design tools and meshing tool. The stage considered for efficiency improvement with the domains and interface is as shown in Fig.2.

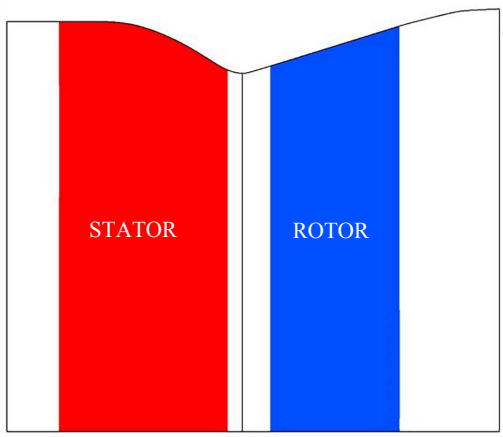

Figure 2: CFD Domain .

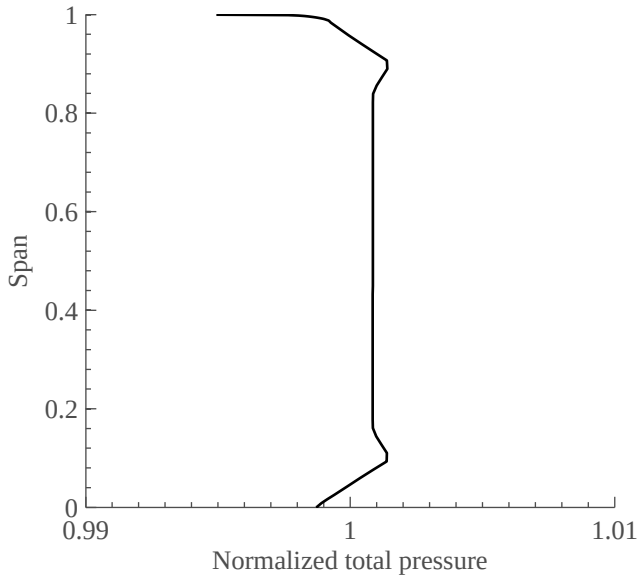

Figure 3: Inlet boundary profile

Mesh Details

Structured hexahedral mesh for the airfoil and flow passage was generated using commercial tool ANSYS turbogrid. Mesh sensitivity study was done for all the design cases. Mesh size was around 3 million for each blade row in the design iterations. Boundary layer was refined with a target y^+ of unity at all wall boundaries. Post analysis numbers for y^+ were maximum of 1 for all the cases at all wall boundaries.

Boundary Conditions

At inlet of CFD domain, stagnation conditions were provided as boundary condition. Total pressure profile imposed at inlet is shown in Fig. 3. This inlet profile was built in comparison to the profile obtained from multistage analysis. At exit of domain, single value of mass flow was used as boundary condition. The purpose was not to impose a static pressure value or profile that would affect the design intent.

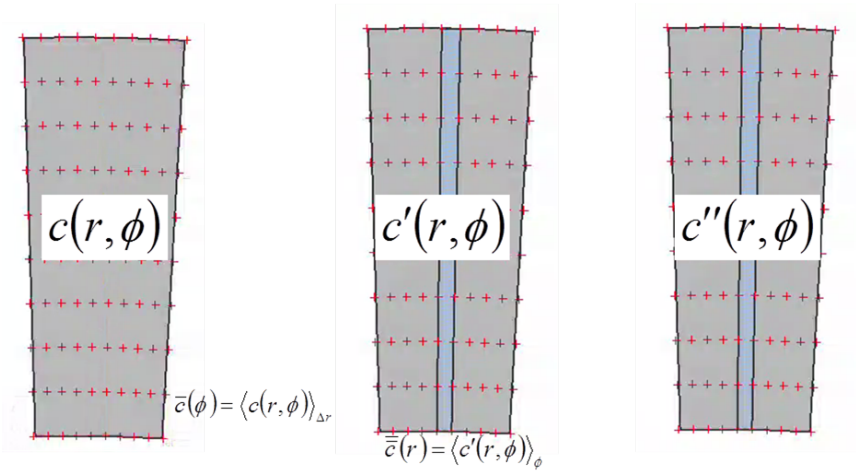

Figure 4: Secondary Kinetic Energy

Objective Functions

Total pressure loss (TPL) considered as objective function is defined as ratio of difference of total pressure at inlet and exit of stator to stator exit dynamic pressure.

$$\text{Total Pressure Loss} = \frac{P_{t(\text{inlet})} - P_{t(\text{exit})}}{P_{t(\text{exit})} - P_{s(\text{exit})}} \tag{1}$$

Secondary losses being the focus in the work done, CSKE and SKEH are used to quantify the improvement in secondary losses. CSKE quantifies the amount of flow deviating from the primary flow direction. There are two definitions of CSKE considered for analyses in present work. One by Germain et al [2] and other by Corral et al [3].

In the method proposed by Germain et al [2], a plane at the exit of stator is considered with velocity field of $c(r,\phi)$ as shown in Fig.4. First $\bar{c}$ is found at each radius by averaging the tangential component. Next step is to find c'. In the field of c' at stator exit, a window from hub to tip of the plane is considered and velocity values are averaged spanwise. This gives $\bar{\bar{c}}$. Difference of c' and $\bar{\bar{c}}$ gives c''. This is considered for all three components of velocity to

calculate secondary kinetic energy. as shown in Fig.4 and in Equation 2

$$\begin{array}{rcl} \bar{c}(\phi) & = & \langle c(r,\phi)\rangle_{\Delta r} \\ c'(r,\phi) & = & c(r,\phi) - \bar{c}(\phi) \\ \bar{\bar{c}} & = & \langle c'(r,\phi)\rangle_{\phi} \\ c''(r,\phi) & = & c'(r,\phi) - \bar{\bar{c}}(r) \\ \bar{c}(r) & = & \langle c(r,\phi)\rangle_{\phi} \\ c''(r,\phi) & = & c(r,\phi) - \bar{c}(r) \\ SKE & = & (mass/2)\{(c''_x)^2 + (c''_\phi)^2 + (c''_r)^2\} \end{array} \tag{2}$$

Definition of CSKE by Corral et al [3] follows the equations

$$CSKE = \frac{(v_i - v_{pi})^2}{v_{\text{exit}}^2} \tag{3}$$

where v_{exit} is the mass averaged stator exit velocity, v_{pi} is the projection of velocity vector at node i over circumferentially mass averaged velocity v_m

$$v_{pi} = \frac{v_i.v_m}{{v_m}^2} \cdot v_m \tag{4}$$

Dot product of two vectors viz. local velocity vector and circumferentially averaged velocity vector is computed. A plane comprising 100 span wise points and 50 tangential points at the exit of stator is considered. Circumferentially averaged velocity direction at each span wise location is considered to be the primary flow direction. At each node point, the velocity vector is compared to the average velocity and the portion of local velocity vector contributing in the primary flow direction is determined by projection of vectors. The remaining portion of local velocity vector is quantified as secondary flow velocity contributing to secondary kinetic energy. This is normalized by nozzle exit dynamic pressure and coefficient is termed as CSKE.

Once the *CSKE* is calculated, procedure to calculate SKEH is as defined by Corral et al [3], wherein the definition of non-dimensional helicity is given by

$$H_i = \frac{v_i.\omega_i}{v_{\text{exit}}^2/c} \tag{5}$$

where v_{exit} is the mass averaged exit velocity, ω_i is the local vorticity vector and c is the blade chord. Finally, SKEH can be written as,

$$SKEH = CSKE_i \cdot H_i \tag{6}$$

Pictorially, helicity can be conceived from Fig.5. The secondary flow image is taken from VKI lecture series by Haller et al [4]. There are two vectors, viz , vorticity vector and velocity

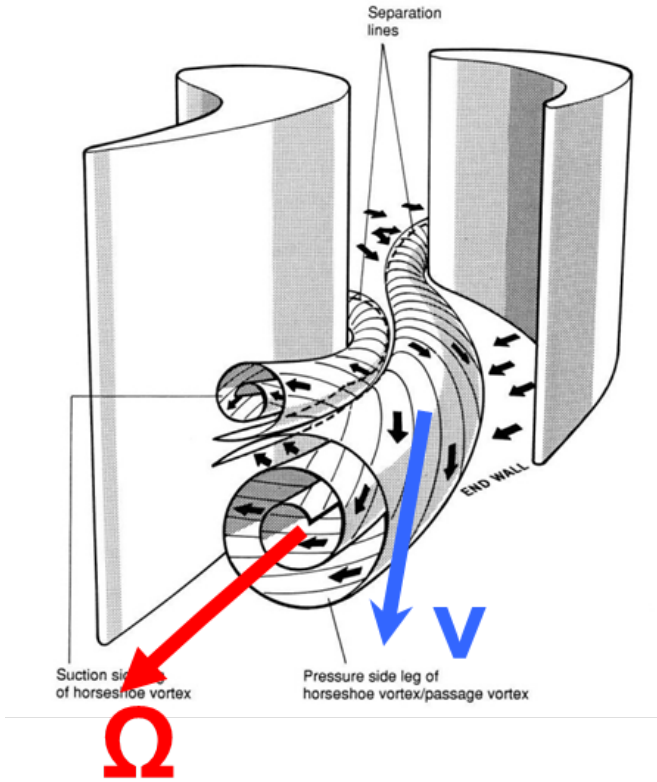

Figure 5: Helicity

vector. If both are aligned to each other, that is the case of streamwise vorticity. If there is some angle between two vectors, the magnitude of dot product is an indicative of relative positions of vectors.

Isentropic efficiency is the third objective function and is defined as ratio of actual enthalpy drop to ideal enthalpy drop.

$$\eta = \frac{h_1 - h_3}{h_1 - h_{3s}} \tag{7}$$

Reduction in Profile Losses

In this chapter, airfoil design for the stator and rotor blade rows is discussed. The objective is to reduce the profile losses and hence increase the efficiency.

The fluid flow in turbomachine can be assumed to be comprising of two components - flow over airfoil sections and flow along the endwalls associated with turning flow in airfoils. The leakage flows add to the complexity and losses to the flow along the endwalls. Local flow behavior on an airfoil section in a turbomachine is influenced by local airfoil section parameters as well as pressure fields existing from adjacent airfoil sections. This is commonly referred to as blade-to-blade flow field. Design of airfoil sections is in turn the design of the flow passage between airfoils because of the strong influence of blade-to-blade flow field. The losses associated with the blade-to-blade flow field is typically coined as *Profile losses*. The discussion in the present chapter is about the airfoil design and associated profile losses specific to the stage under consideration i.e. the stage from intermediate pressure section of SST-900.

From the stagnation point at the leading edge, the flow starts from zero velocity and boundary layer starts growing as shown in Fig.6a. The figure highlights the suction side of the airfoil because more than 80 % of the losses occur on the suction side of the airfoil in turbine flows [5]. Initially, the boundary layer is laminar. The changes in the boundary layer are significant and contribute towards loss patterns. In order to reduce skin friction loss on the suction side, the fraction of laminar boundary layer length has to be increased to the maximum possible extent. This is because, it is reported that the friction loss is proportional to the square of velocity in the laminar region and to the cube of velocity in the turbulent region [6]. A laminar boundary layer, however, stands a risk of separation bubble towards the trailing edge of airfoil because of increased diffusion factor. Hence, such profiles should be carefully designed to ensure turbulent reattachment before reaching the trailing edge. Shape factor is a non-dimensional parameter which is indicative of the location of transition point. A sudden dip in the value of shape factor shown in Fig.6a indicates the transition point.

For given boundary conditions of inlet and exit Mach numbers, a turbine airfoil can be designed to be either a front-loaded airfoil or an aft-loaded airfoil. Front-loaded airfoils are also called to be flat-roof-top designs owing to the Mach number distribution on the

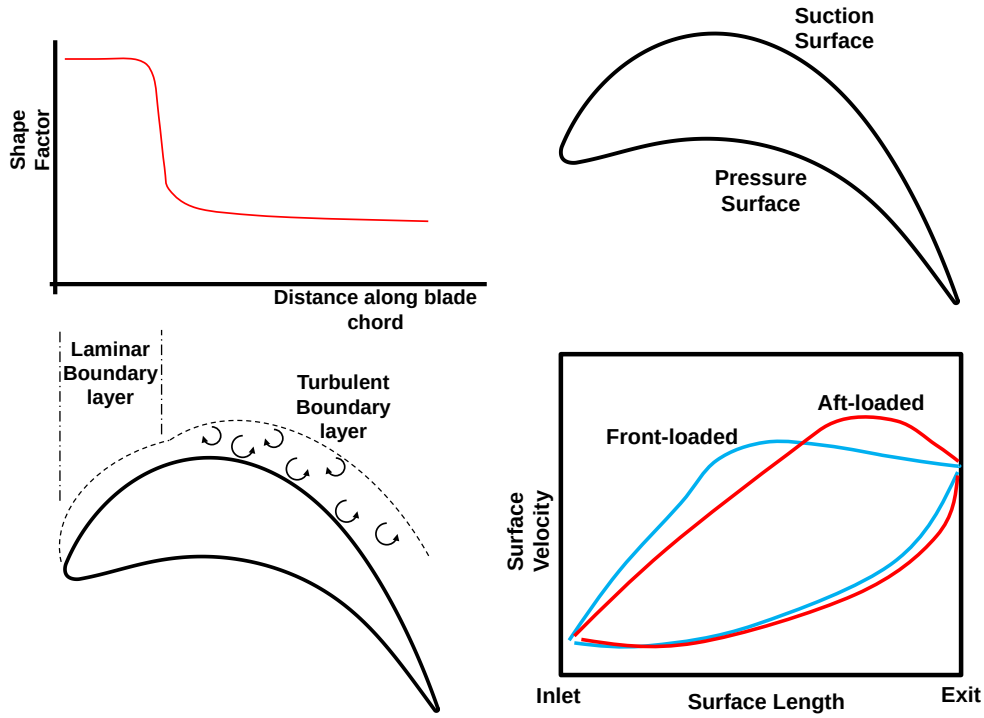

(**a**) Schematic of flow over airfoil

(**b**) Front-loaded and aft-loaded airfoils

Figure 6: Flow over airfoil

suction side. A schematic representation of airfoil designs is shown in Fig.6b. The decision for an airfoil to be front-loaded or aft-loaded depends on free stream Reynolds number, amount of expansion in the blade-to-blade passage and boundary layer patterns on the airfoil. Extent of profile loss numbers are vastly dependent on the path taken by surface velocity distributions from inlet Mach number to exit Mach number as shown in figure. Coull et al [7, 8] studied the effects of front-loaded and aft-loaded airfoils on profile losses of turbine blades. It was reported that front-loaded airfoils are more robust for various incidence angles. However, in both the designs, loss is a strong function of diffusion factor. Diffusion factor is a measure of diffusion gradient in the blade-loading diagram. Experimentally, it was observed that front-loaded airfoils cause higher secondary losses [9]. Even the leakage losses increase with front-loaded airfoils [10]. These factors further add to complexity of design philosophy for optimum airfoil loading.

Dependence of airfoil section performance on the incidence angle is another aspect that is analyzed in present work. Effect of incidence angle on the profile loss is reported by many researchers [11–13]. Effect of incidence is also mentioned in prediction models proposed

by Moustapha et al [14]. The general conclusion drawn from these reports is, profile losses increase quite rapidly as the incident flow vector tends to move from the pressure side of airfoil towards the suction side of airfoil. As this process takes place, a separation bubble starts to form on the pressure side of airfoil and causes gradient of loss with incidence angle. In the context of present work, changes in flow behavior towards the leading edge is one of the points to focus.

High performance airfoil designs require good control on the curvature distribution on airfoils. Effect of smooth curvature on airfoil performance is discussed by Korakianitis et al [15, 16]. The curvature and the slope of curvature are highlighted as controlling parameters to avoid undesirable loading distributions, local acceleration and deceleration. The curvature controls the local flow velocity levels. Theoretical and experimental evidences are provided for dependency of blade performance on curvature distribution of the airfoil. When comparing the difference in performance between designed blade and actual manufactured blade, curvature and its slope being maintained rather than every point being maintained, is projected as an important aspect.

The primary research objective here is to decide design philosophy for stator and rotor airfoils i.e. front loaded or aft-loaded. The Reynolds number for the present geometry being high ($> 1 \times 10^6$), the design philosophy is not obvious and needs to be established for the geometry considered. The degree of reaction being low is another factor to be considered. Designing better airfoils for the stage also means addressing issues like incidence and curvature distribution if any.

In the work presented here, modifications made to airfoil sections of stator and rotor are discussed. To begin with, modifications made to rotor airfoil are discussed.

Improvements in Airfoil Design

Rotor Redesign

From the non-dimensional numbers that define the stage parameters i.e. work coefficient, flow coefficient and reaction, the flow angles and velocity vectors were first calculated. The velocity triangle which serves as input to airfoil design was first checked. The velocity triangle calculated is shown in Fig.7a. The values of the velocities are not shown for proprietary reasons. The focus here is on the rotor inlet flow angle. The calculations show that there is difference in the rotor inlet flow angle and the rotor inlet metal angle. In the figure, calculated flow angle and actual metal angle are shown to be $38.82°$ and $35.27°$ respectively. There is a negative incidence of $3°$. This being negative incidence, the first objective was to check for efficiency gain by correcting the incidence. Rotor inlet metal angle was corrected

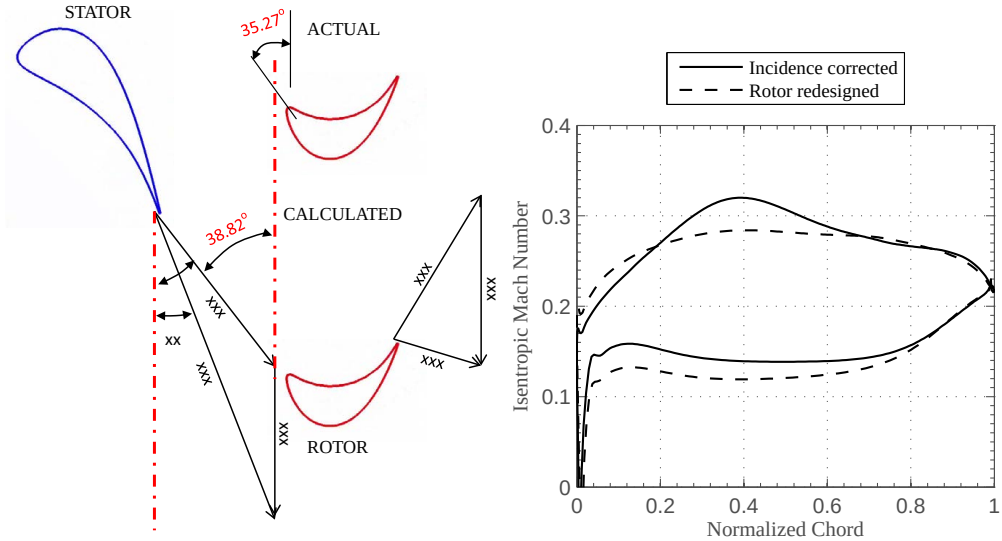

(**a**) Velocity Triangle

(**b**) Blade Loading at 50% span

Figure 7: Blade loading comparison

by 3° to match the incident flow angle. Elaborate results and methodologies from this study are presented in Paper I. It was observed that due to change in incidence, a gain in total a total stage efficiency of 0.17 % could be obtained.

Fig.7b shows the blade-loading for rotor with incidence corrected. It can be observed that from the leading edge there is initial acceleration to Mach number 0.32 at a distance of 0.4 axial chord. And from there on, flow is diffusing to exit Mach number. The reaction of the stage being low, the expansion of flow in the rotor is relatively less. Hence the acceleration to 0.32 Mach number and then the diffusion could be avoided. This was attempted and result is shown in Fig.7b. The redesigned rotor shows flat top Mach number distribution with reduced peak Mach number. With the Mach number levels reduced, the losses are also reduced. With the rotor redesigned, the stage efficiency further increased by 0.06 %. Observing the streamwise vorticity distribution at the exit of rotor, it was verified that the improvement was only from profile losses and there was no changed in the secondary loss pattern due to changes in rotor redesigns. Overall increase in efficiency due to rotor airfoil redesign was 0.23 %.

Stator Redesign

As the reaction of the stage under consideration is low, relatively higher acceleration can be expected in stator. The blade-loading of the baseline stator is shown in Fig.8a. It can be

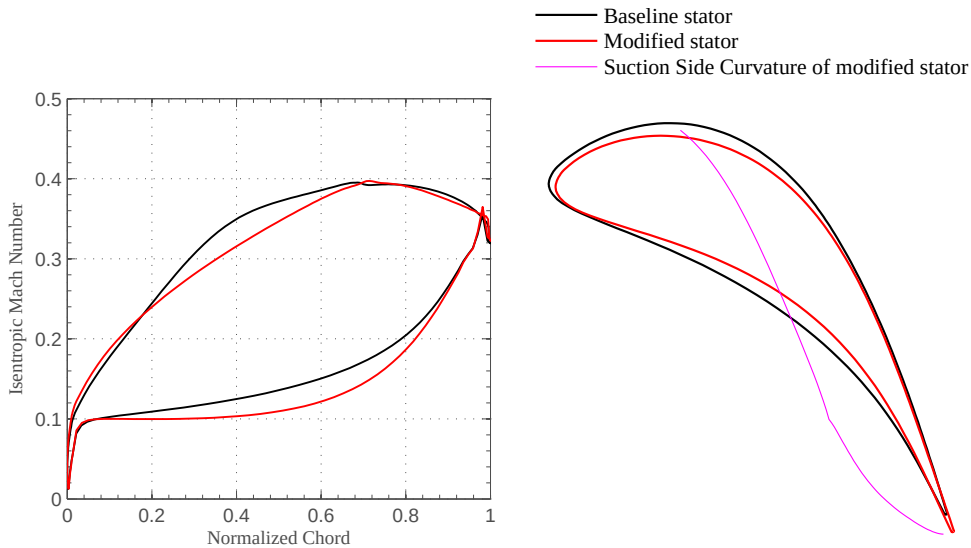

(**a**) Blade Loading at 50% span (**b**) Airfoil Comparison

Figure 8: Modified Stator Design

observed that the baseline stator has two slopes of acceleration on the suction side. With an intent to make the acceleration smoother and to make the flow accelerating till further downstream on the airfoil surface, stator was redesigned. The overlap of resulting blade-loading over baseline blade-loading is shown in the figure. The acceleration is more gradual and smooth in the redesigned stator. Also, the airfoil is relatively more aft-loaded. In the redesigned stator, the shape factor was checked for laminar to turbulent boundary layer transition. As a result of redesign, the transition from laminar to turbulent boundary layer is delayed. These two aspects of gradual acceleration and delaying the transition are favorable to reduce the profile losses. However, it can be noted that the diffusion patterns in the baseline and the redesigned stator are similar. Another important factor contributing in the redesigned stator is the curvature distribution. The baseline airfoil, the redesigned airfoil and the curvature distribution on suction side of redesigned airfoil are shown in Fig.8b. The curvature is maintained smooth on the suction side of modified airfoil. The total to total stage efficiency of the stage further increased by 0.1 % due to changes in the stator airfoil design.

Summarized improvements in total-to-total stage efficiency due to airfoil modifications of stator and rotor airfoils are shown in Table 2. Significant improvements can be seen due to incidence correction in rotor; 0.6 in total pressure loss (C_{pt}) and 0.17 points in efficiency. Changes in airfoil design for stator and rotor resulted in overall efficiency improvements of 0.33 %

Table 2: Accumulated improvement in performance

Modifications	C_{pt}^{Stator}	C_{pt}^{Rotor}	$\Delta\eta$
Rotor incidence correction	0.0	0.6	0.17
Rotor redesign	0.0	0.8	0.23
Stator redesign	0.14	0.0	0.33

Performance with modified pitch-to-chord ratio

In turbomachines, as mentioned, there is a strong influence of adjacent airfoil section on the blade to blade flow field rather than flow over blade in isolation. This flow field is strongly influenced by the pitch-to-chord ratio. Fig.9 shows the definition of pitch-to-chord ratio and typical trends in loss behavior depending on pitch-to-chord ratio. It can be understood from the figure that an optimum pitch-to-chord ratio is a break even between viscous and turning losses. Higher the number of blades (low pitch-to-chord ratio), higher is the wetted region and higher is the viscous loss. With the pitch-to-chord ratio being low, there is a possibility of redundancy of metal used.

Lower the number of blades, higher is the lift force per airfoil section for fixed boundary condition. Due to less number of blades, the lift force per blade increased and hence velocity levels are higher. These factors lead to higher losses. An optimum pitch-to-chord ratio is a choice of the designer for minimum losses. During the initial design phase, there are loss models to select the pitch-to-chord ratio [17–21]. The loss models help the designer a great deal to select the preliminary pitch-to-chord ratio. However, enough care should be taken at later design phase to check for performance with selected pitch-to-chord ratio.

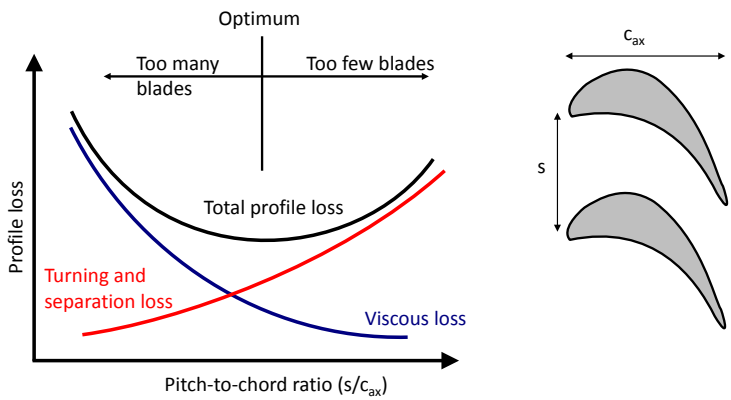

Figure 9: Pitch-to-chord ratio .

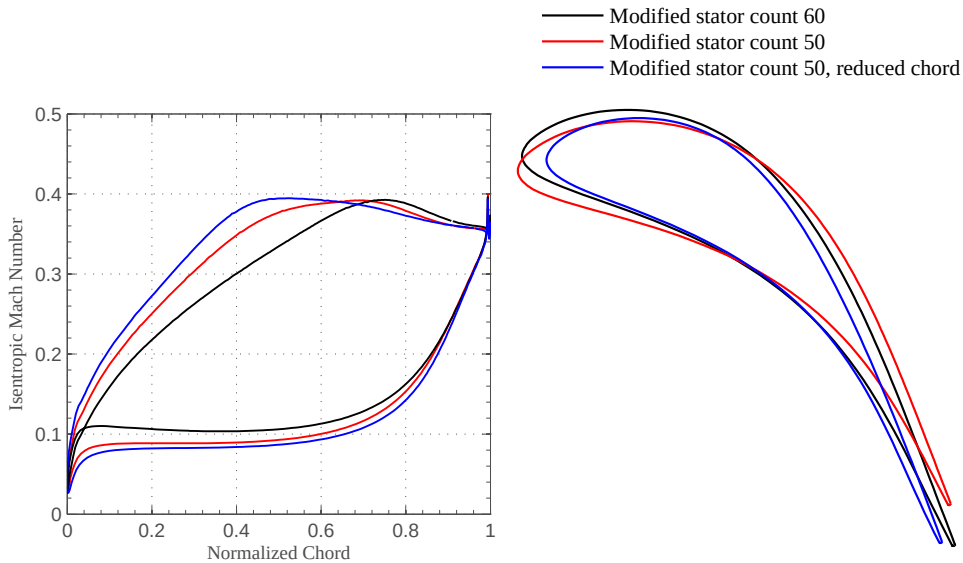

(a) Blade Loading with modified s/c

(b) Airfoil Comparison with modified s/c

Figure 10: Pitch-to-chord study for stator

Pitch-to-chord ratio of Stator

Performance improvements in stator by modifying the pitch-to-chord ratio was done in two steps. First, the blade count was reduced from 60 to 50 where in the pitch-to-chord ratio increased from 0.75 to 0.82. Second, the pitch-to-chord ratio was further increased by decreasing the axial chord by 3 mm. Final pitch-to-chord ratio of the stator that was studied was 0.86. The blade-loading comparison for the three cases are shown in Fig.10a. Since the boundary condition was maintained, it can be observed that blade-loading increased with each iteration of increased pitch-to-chord ratio. The area covered by the blade-loading curves on the suction and pressure side is indicative of the lift force or the work done by the airfoil section. This area covered by blade-loading curve can be seen to increase by increase in pitch-to-chord ratio. The location of peak Mach number shifts upstream on the suction side of the airfoil. This shift in peak Mach number also means that there is relatively larger surface length available for the flow to catch up to the exit Mach number. Hence reducing the diffusion losses. The total-to-total efficiency of the stage increased by 0.52 % with the reduced blade count and further increased to 0.66 % with decreased chord. These efficiency numbers include the airfoil design iterations that were discussed in previous sections of this chapter. The comparison in airfoil sections are shown in Fig.10b. The increase in efficiency indicated that the airfoil section can still handle the turning for the given boundary condition.

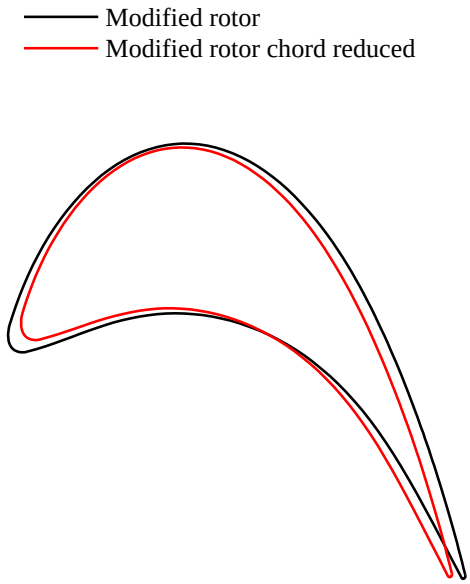

Figure 11: Pitch-to-chord study for rotor

Pitch-to-chord ratio of Rotor

Pitch-to-chord ratio variation in rotor is more complicated as the mechanical requirements are more stringent in rotating parts. Hence, not many modifications were tried on rotor. Axial chord of the rotor was reduced by 2 mm while retaining the blade count. Comparison of airfoils is shown in Fig.11. Overall efficiency gain with airfoil improvement and pitch-to-chord ratio study on stator and rotor was 0.74 %

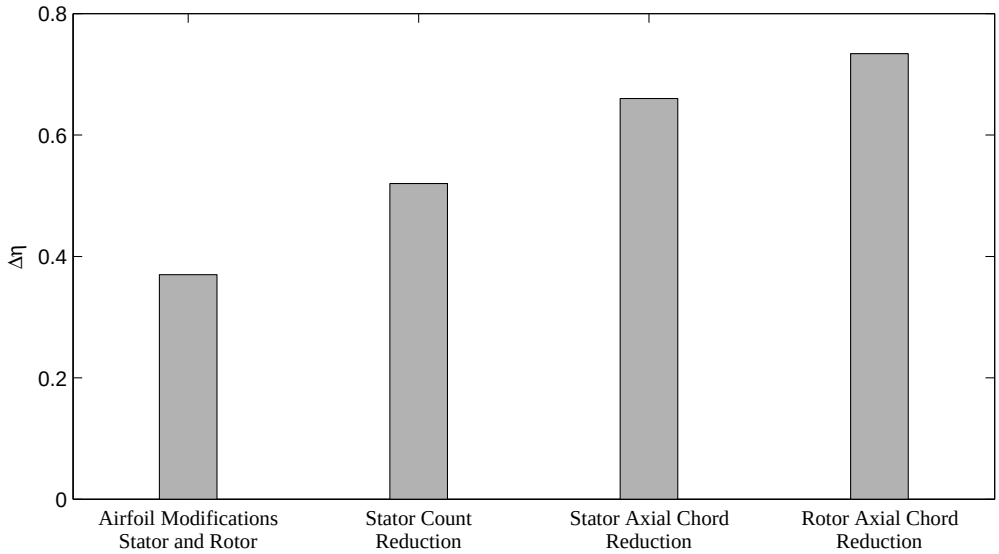

Figure 12: Efficiency gain with airfoil redesign

Summary

The efficiency improvements due to redesign of airfoil sections for high aspect ratio blades were found to be significant. The overall improvement is 0.74 %. Fig.12 shows the incremental improvement in efficiency by each design iteration performed. This improvement, verified numerically by RANS simulations is significant for the design to be relooked at. It is understood that these numbers that are being looked at aerodynamic perspective, needs to be endorsed by other disciplines too. But the amount of efficiency improvement makes a strong case to be looked at from product perspective.

Reduction in Secondary Losses

Secondary loss is the target area discussed in this chapter which arises due to secondary flows. Any flow behavior not complying to primary (expected) flow behavior is termed as secondary flow behavior. In turbomachinery flows, the flow is expected to follow the airfoil guided path. This flow is termed as primary flow. Flow that deviates from the path guided by airfoil is the secondary flow. One of the main causes for secondary flow is the embedded vorticity in the incident total pressure profile impinging on the turbine airfoil along the blade height. Vortex lines tends to be stretched on pressure side and suction sides of airfoil giving rise to horse-shoe vortices. These horse-shoe vortices interact with the expected primary flow and generate secondary loss mechanism. Amount of secondary loss is a function of many geometrical parameters such as aspect ratio of blade, turning on the blade, pitch-to-chord ratio and also the boundary conditions.

During the present work, an attempt was made to reduce the secondary losses in the turbine stage considered. Vortexing methods and leaning of airfoil are well known three-dimensional modifications on the blade row to reduce secondary losses. Both these design modifications are discussed for the stage under consideration. Along with the non-intruding design modifications, intruding design modification like the boundary layer fence was also attempted. Introduction of boundary layer fence was based on hypothesis of breaking down horse shoe vortices.

Quantification of improvement in secondary losses was a challenge and a parameter Secondary Kinetic Energy Helicity was formulated from the available literature. SKEH and co-efficient of secondary kinetic energy discussed in the chapter *Numerical Methods* were the two functions used to monitor secondary losses for the design modifications considered.

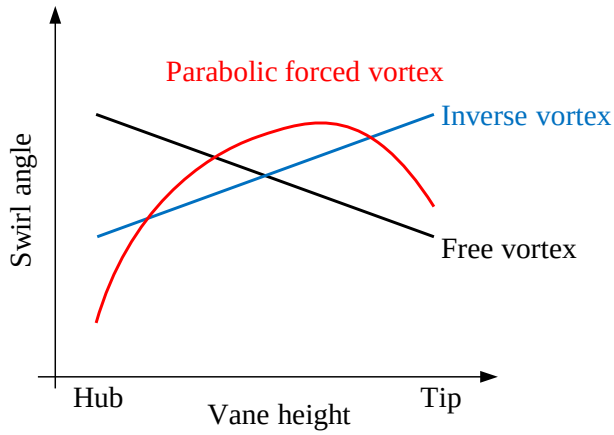

Figure 13: Vortexing philosophies.

Vortexing

Vortexing methods primarily aim at reducing secondary losses. Also, there have been extensive research on using vortexing to produce desired pressure profiles at stator exit [5]. These desired pressure profile affects the radial distribution of reaction and can affect the leakage loss. Hence, vortexing influences the work and spanwise properties of a stage. Fig.13 shows three stator exit swirl philosophies - free vortex, inverse vortex and parabolic forced vortex. Free vortex design is a result of conservation of angular momentum [22]. In inverse vortex design, the intention is to aim at less expansion in stator at hub and more expansion at stator tip. The inverse design type resembles the forced vortex approach and the difference lies in the lower swirl angle variation. One important feature of the inverse vortex design is the rotor hub inlet angle, where one can show a significant reduction in gradient of incident swirl angle. The inverse vortex design also results in a fairly un-twisted rotor leading edge. The latter is indeed useful for cooled gas turbines but this is outside the current research work. The gain in efficiency due to the inverse vortex twist may be accounted to the reduced turning at the hub-section for both the stator and rotor.

Parabolic forced vortex aims at less expansion at hub and tip section. This is because the incoming flow in the boundary layer has embedded vorticity and less momentum at hub and tip. To maintain the same reaction and same work extraction, this calls for more expansion at the mid-section. These options are shown in comparison to free vortex design in Fig.13 which is reproduced from the book by Japikse et al [23]. It is clear from the figure that, for a parabolic forced vortex design, flow angles are reduced at the endwalls. This results in opening up of airfoils for a given pitch and hence increasing mass flow rate across endwall sections. As a consequence, flow angles at mid span increases and throat area reduces. This reduces the mass flow at mid-section. So, parabolic forced vortex changes the mass flow

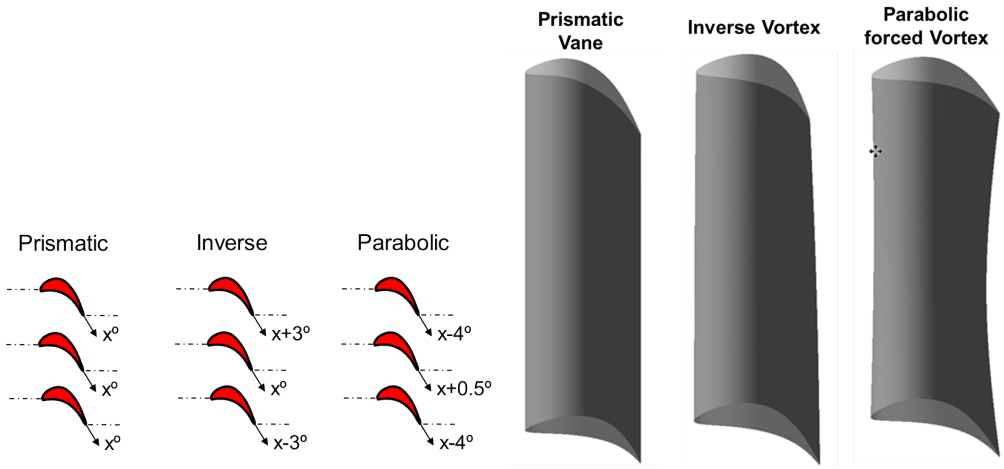

(**a**) Schematic of angle representation for vortexing (**b**) Stator Designs

Figure 14: Vortexing Designs

distribution from hub to tip and thus affects efficiency.

Implications of vortexing on the Stage considered

The three discussed vortexing methods were attempted on the stage considered. Fig.14 shows the design modifications on the stator in order to arrive at the desired vortexing method. The angles shown use tangential reference angles i.e. angles are measure positive clockwise from the axis of the blades. For inverse vortex design, midspan section was retained as it is. Tip section was closed by 3°and hub section was opened by 3°. For parabolic forced vortex design, both hub and tip sections are opened by 4°each and mid span section is closed by 0.5°. These airfoil section rotations are shown in Fig.14a. Visual differences in three stator configurations can be seen in Fig.14b. Number of blades and hence the pitch was retained the same as in reference stator. With the constraint that flow coefficient, work coefficient and reaction of the stage to be the same as in baseline, the challenge was to maintain the same throat areas for all stator configurations. Both the stator configurations matched the reference stator area within 0.3 % difference. Design modifications and airfoil creations were done using inhouse airfoil design tool. Throat area measurement was done using commercial CAD tools. For all the three cases analyzed, rotor was retained the same. Rotor is again a prismatic airfoil for baseline case. Using the same rotor for all the cases is expected to have incidence problems. But, the focus of present work is vortexing in stator.

The total pressure losses in stator reduced by 1 % in inverse vortex design and 0.5 % in parabolic forced vortex design. SKEH reduced by 6 % in inverse vortex design and 5 % in parabolic forced vortex design. The designs show reduction in secondary losses. However,

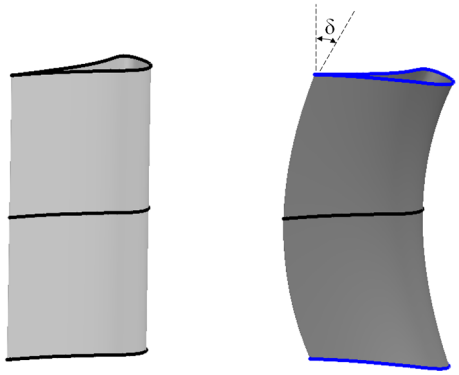

Figure 15: Compound lean design of stator.

the total-to-total efficiency numbers does not reflect the losses reduced in the stator blade row.

Compound Lean

Three-dimensional shaping of stator to reduce losses in a turbine stage has a long history [24]. Straight lean, compound lean, sweep, localized blade twists are a few modifications to mention [25]. Though the exact working principle of lean is not clear yet, a very good theoretical perspective is conveyed by Denton summarizing the most important effects and explanations available [25]. The effect of pressure side leaning towards the endwalls is primarily to increase the pressure locally and hence push the flow towards the midspan of airfoil where the flow is predominantly following the airfoil. If in stator, lean is incorporated at both endwalls, the configuration is termed as *compound lean*. As a consequence, lower loadings at endwall can be obtained.

Efficiency improvements in turbine stage due to compound lean in stator is discussed by researchers [26–28]. These reports show significant improvement in stage efficiecy due to compound lean on stator. However, recently there have been few publications by Rosic et al [29] reporting no gain in efficiency with compound lean. With the diverse reports and opinions about compound lean and with the task of efficiency improvement of stage of an industrial turbine, the rational thought not to give out any opportunity in efficiency improvement is to implement compound lean and analyze. Same is done in present study.

The compound lean design of stator is shown in Fig.15. The angle δ shown in figure is the measure of amount of compound lean. Two values of δ were incorporated in the study-

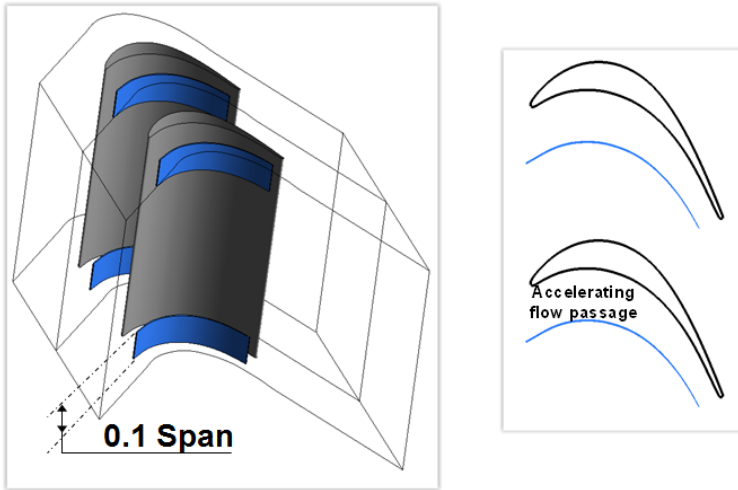

Figure 16: Schematic representation of boundary fence.

15°and 30°. With the numerical analyses of the stage, it was found that the secondary losses were reduced significantly at the exit of the stator. The coefficient of secondary kinetic energy reduced in compound lean configuration by more than 30 %.

All the effects of compound lean reported in literature like off-loading of endwall sections and migration of flow towards the midspan region could be captured by numerical approach. However, the efficiency gains to the magnitudes reported in literature, due to compound lean could not be achieved. The results obtained were more in line with the results presented by Rosic et al [29]. Improvements in flow reflecting in total-to-total efficiency could not be seen. There could be two reasons for losses not reflecting in improvement in efficiency. One, advantage obtained in stator blade row is nullified by the addition of losses in rotor blade row or two, may be a limitation in the prediction methodology adopted. Since the experiments by Rosic et al [29] also showed similar trends as obtained in present work, it makes a stronger inclination towards the gain in stator blade row has resulted in addition of losses in rotor blade row.

Boundary Fence

Boundary fence is a design configuration which intrudes into the flow path to reduce the major secondary loss mechanisms. Fig.16 shows typical boundary fence that was tried on T106 cascade for study purpose. This cascade was chosen from open literature. The selection of boundary fence is based on two hypotheses. First hypothesis is to cut the vortex line incident on the blade row and hence reduce the strength of the horse shoe

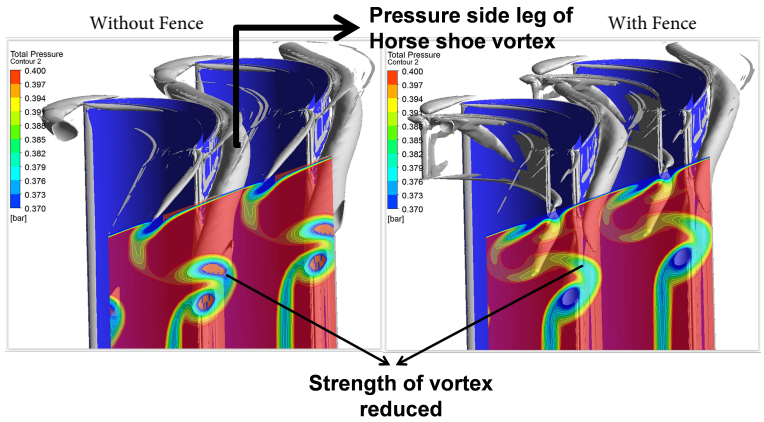

Figure 17: Reduction of vortex strength by boundary fence.

vortices. Second is to reduce the cross flow between airfoil due to blade-to-blade pressure field.

Coefficient of secondary kinetic energy and SKEH evaluation of the design modification showed significant improvement in secondary losses. CSKE reduced by 30 % and SKEH reduced by 40 % in the presence of boundary fence. Total pressure loss also decreased indicating that added loss due to intrusion in flow path does not surpass the gain obtained due to reduction in secondary losses. Fig.17 shows the total pressure loss contour at the exit of the cascade overlapped with the vortex structures. Reduction of vortex strength in presence of boundary fence can be observed.

Flow path modifications

The domain of the target stage is shown in Fig.18 for reference. Axisymmetric endwall contouring incorporated at the casing in the baseline flowpath shown is historically referred to as Russian kink. Main task here is to assess the significance of endwall contouring on the performance of the stage. Given the three main loss mechanisms in turbomachinery flow *viz* profile loss, secondary loss and tip leakage loss, understanding as to which component is being addressed by the presence of endwall contour in the present target stage is sought.

Static pressure changes that can be induced by curving the streamlines in meridional direction is one of the avenues to influence local loss mechanisms. Endwall contouring is one such design modification. To authors' knowledge, endwall contouring was first introduced by Deich et al [30]. The purpose of axisymmetric endwall contouring was to create a local radial pressure gradient in the meridional plane. This phenomenon of affecting the pressure by axisymmetric and non-axisymmetric endwall contouring is studied extensively [31–34]. The spanwise pressure distribution at stator exit also affects the tip leakage losses and can be used to reduce the same. As a consequence, the reaction gradient for the entire stage can be reduced using endwall contouring.

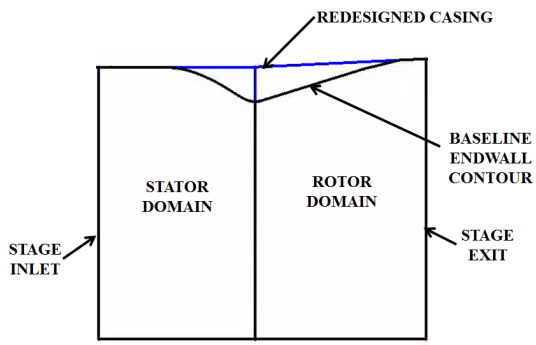

Figure 18: Flow path modification.

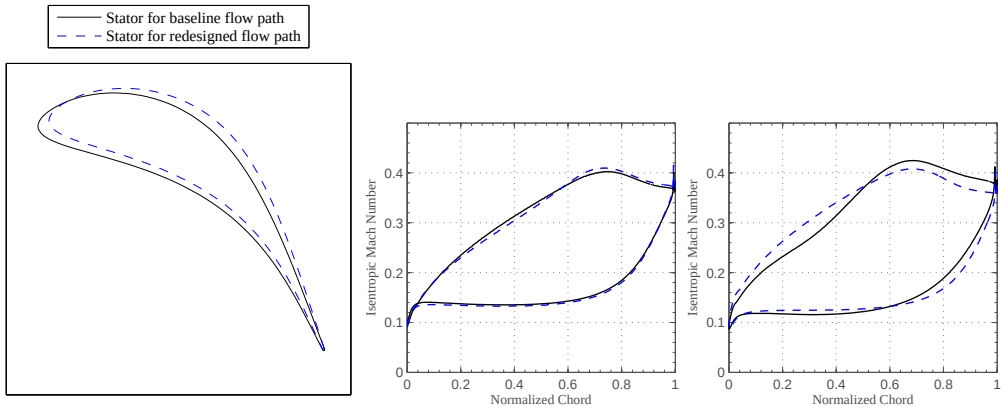

(**a**) Stator airfoil for new flow path (**b**) Blade Loading at 50 % span (**c**) Blade Loading at 90 % span

Figure 19: Blade loading comparison

Flow path modification

Design parameters of turbine stage being retained, redesign of the flow path to remove endwall contouring in the tip region is done. In order to maintain the stage loading and the degree of reaction, turning on the stator and rotor is increased. The changes in the flowpath are made from a retrofit point of view, i.e inner and outer radii at the stage inlet and the stage outlet are retained so that the stage fits into the flow path with upstream and downstream stages. This also enables design verification in multistage environment. Airfoil sections developed in earlier chapters are considered. The stage with modified airfoil design is considered as baseline for flowpath study. Throat areas of stator and rotor for new flow path are reduced in order to match the reaction. Degree of reaction was matched by trial and error and verified by three-dimensional viscous CFD analyses. To represent the distribution of local pressure at stator exit, a term non-dimensional static pressure is used which is defined as

$$\text{Non-dimensional Static pressure} = \frac{P_s}{P_{t(\text{inlet})}} \tag{8}$$

Endwall contour on the baseline flowpath was removed. Comparison of baseline flowpath and modified flow path is shown in Fig.18. Stage design parameters were retained from baseline. The annulus area after the stator in the flowpath is increased in the modified flowpath. Hence, the bulk velocity levels are reduced. In order to maintain the same reaction, the velocity level had to be increased. This was achieved by closing the stator by 2°. Airfoil profile thus obtained is shown in comparison with the baseline stator in Fig.19a. As the baseline airfoil is rotated by certain amount, axial width of the airfoil is reduced. This rotation affects the blade-loading on the stator airfoil.

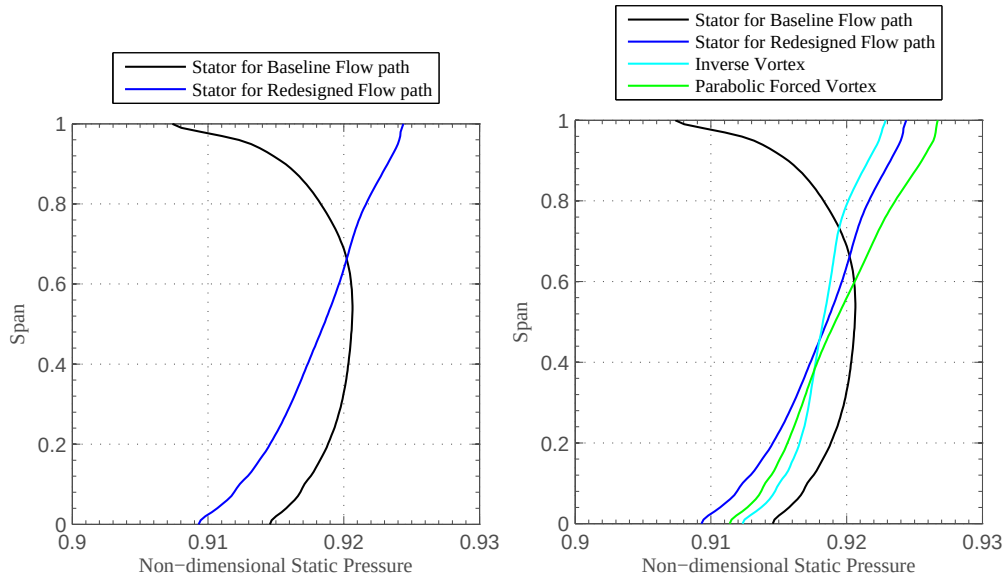

(**a**) Non-dimensional P_s - Stator exit

(**b**) Non-dimensional P_s - Stator exit- Vortexing

Figure 20: Vortexing Designs

Comparison of blade-loading at the midspan of stator blade row is shown in Fig.19b. Movement of throat point on the suction side of airfoil due to closing of airfoil was less than 1 % of axial chord. This was calculated and verified using CAD tools. Because the throat point movement on the suction surface is relatively less, the location of peak Mach number is almost the same for both baseline and the new stator without endwall contouring. Since the downstream pressure levels and Mach numbers are fixed from baseline, there is not much difference in the blade-loading patterns at midspan. The peak Mach number for new stator is slightly higher than the baseline case at midspan.

Since the endwall contouring was removed in the tip region, blade-loading plots are also compared at tip region for the stator in Fig.19c. Blade-loading in the baseline case is relatively higher by virtue of reduced pressure at stator exit because of endwall contouring. Endwall contouring is typically done to reduce blade-loading towards endwall. The fact that blade-loading is increased in this case is due the axial position of the endwall contour which drives low pressure being present at the stator exit tip location.

One of primary reasons for the presence of endwall contour in baseline flow path is to obtain desired pressure profile at the stator exit. The pressure profile in turn controls the leakage flows and hence the leakage losses [5]. Static pressure profiles at the exit of stator in the form of non-dimensional static pressure are shown in Fig.20a. Local reduction in pressure in presence of endwall contour is evident in the baseline flow path case at the tip.

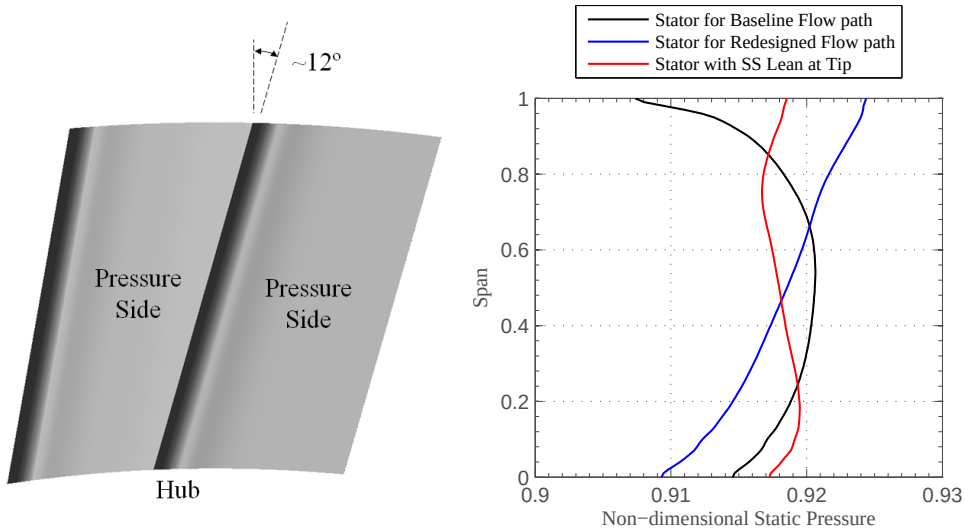

(**a**) Stator Design

(**b**) Non-dimensional P_s - Stator exit- -SS Lean at Tip

Figure 21: Suction Side Lean at tip

In case of new flow path, static pressure value at the tip is increased and hence, increasing the pressure difference across the tip seal region. This is not favorable as the leakage flow increases with higher pressure gradient.

In order the reduce the pressure locally with the redesigned flowpath, vortexing was incorporated in the stator. Vortexing methods adopted were in line with the philosophies discussed in chapter 4. It can be observed from Fig.20b that low pressure as obtained by endwall contouring could not be obtained by any of the vortexing methods attempted.

It is well understood and explored phenomenon that leaning the stator with pressure side towards endwall would increase the pressure locally [25]. A counter thought to this fact would be, to lean suction side towards endwall to reduce pressure locally. This was attempted with suction side lean designed at the tip. This is termed as negative lean in literature. Advantages and disadvantages of negative lean are reported by Haller et al [4]. In the context of present work, negative lean is used to decrease the pressure values locally at stator exit tip.

After several iterations, configuration shown in Fig.21a was obtained. This was done by tangential movements of airfoil sections resulting in suction side lean angle of 12 degrees at the tip. With the suction side lean at the tip, spanwise distribution of pressure at exit of stator was extracted and compared with the previous results. Comparison is as shown in Fig.21b. The static pressure gradient is further reduced when compared to the vortex-

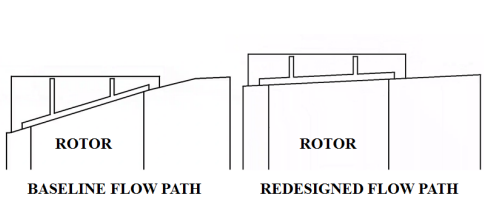

(**a**) Tip Shroud Configuration

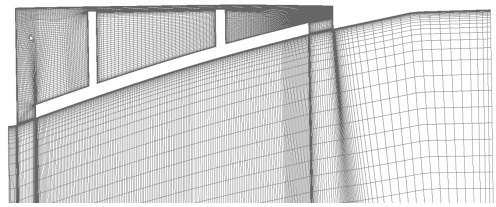

(**b**) Tip Shroud Mesh

Figure 22: Tip Shroud Study

ing methods, to the extent that static pressure has nearly a constant value from root to tip. By introducing suction side lean at tip, pressure side leaning in the hub region evolves as a consequence. This pressure side leaning at hub adds to already existing straight positive lean at hub which in turn assists in reducing the spanwise static pressure gradient. With the changes in the flow path and the stators discussed, isentropic total to total efficiency numbers were extracted and compared. Close to $0.2\,\%$ improvement in total-to-total efficiency can be shown by changing the flow path.

Tip Shroud Implementation

With the significance of stator exit static pressure profile discussed earlier with reference to tip leakage losses, it is important to check the performance of the modifications with tip shroud. Two tip shroud configurations were considered, one for baseline flow path and other for modified flow path as shown in Fig.22a. These were designed purely from a study perspective and has no similarities to geometry in actual turbine stage. Tip clearance was maintained to be the same in both the cases. The thought to retain the tip clearance distance rather than tip clearance area was to consider mechanical constraints to maintain gap between rotating and non-rotating components to avoid rubbing. Two seal strips were considered. It is reported that the tip leakage losses decrease by increase in number of seal strips [35]. For ease of meshing and numerical calculation, two seal strips were finalized. Also, since the difference in performance numbers are reported, it is assumed that number of seal strips will not have impact on the conclusions.

Rotors were meshed along with tipshroud using ICEMCFD. Hexahedral mesh was generated without interface between rotor and tipshroud geometry. y^+ of unity was targeted at all wall boundaries. A typical tipshroud mesh is shown in Fig.22b. The outer walls of the tipshroud i.e. the tip cavity was defined as stationary wall in the analysis.

With the tip leakage flow modeled, difference in efficiency numbers are shown in Fig.23a. CFD was done with stator and re-meshed rotor with tipshroud. Delta efficiency values

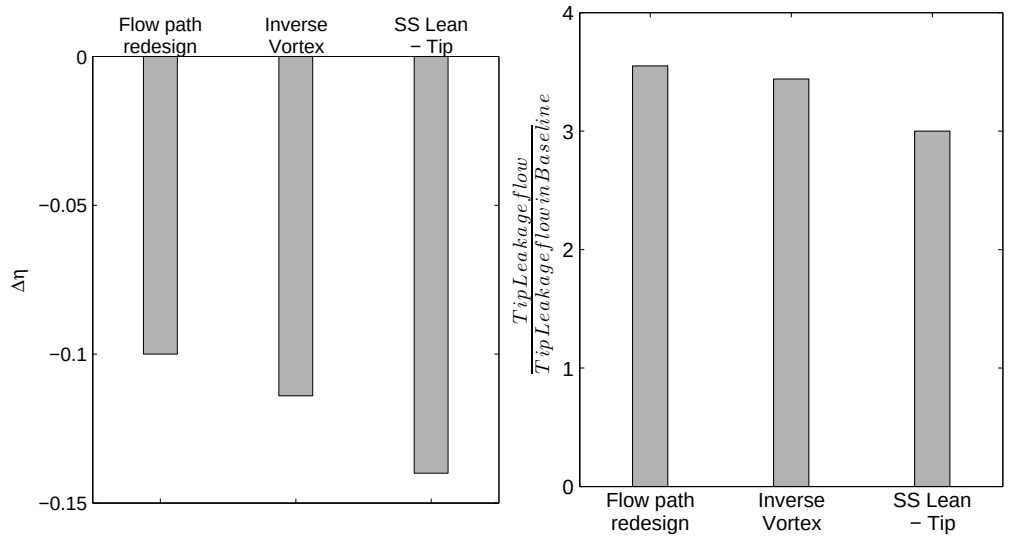

(**a**) Efficiency with tipshroud

(**b**) Tip leakage flow comparison

Figure 23: Performance - Tip Shroud

with reference to baseline case with tip shroud are shown. Efficiency numbers of new flow path and corresponding stator modifications are less than the baseline flow path with tip shroud. There is a change in scenario in terms of efficiency numbers with and without tip leakage in the analyses. Efficiency numbers of baseline flow path with tip shroud is better than the other modifications attempted.

In order to understand the effect of stator exit pressure profile on the tip leakage flow, the leakage flow values were extracted from numerical analyses and plotted in Fig.23b. Tip leakage flow in the baseline flow path case is around 0.25 kg/s and this is taken as reference. The leakage mass flow is approximately $0.2\,\%$ of the primary mass flow through the stage. Other tip leakage flows are shown as multiples of reference case. Tip leakage flow increased with the increase in pressure at the tip of stator exit. It can be observed that low pressure at the tip in baseline case has a significant effect on the leakage flow. Also, the modifications to reduce the pressure at the tip does not reveal significant impact on the tip leakage flow.

To segregate if the penalty in efficiency is by virtue of tip leakage loss alone, the indications from secondary losses had to be studied. For this reason, spanwise distribution of streamwise vorticity direction at the stator exit for the cases analyzed are extracted in Fig.24. Streamwise vorticity is calculated using the equation

$$\omega_{streamwise} = \omega_{axial} \cdot \cos(\alpha_2) + \omega_{tangential} \cdot \sin(\alpha_2) \tag{9}$$

In the flow path and stator modifications attempted, vorticity values have either decreased

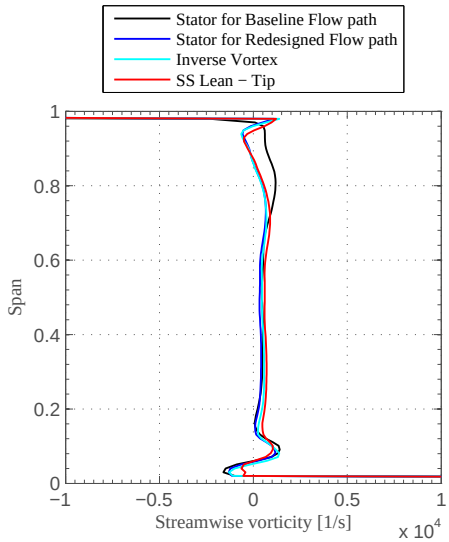

Figure 24: Streamwise vorticity - Stator exit

or remained at same levels as the baseline case. This indicates that the loss in efficiency in the modified cases is a strong function of tip leakage loss.

To reconfirm the effects of stator exit static pressure profile, another check with CFD analysis was done. Stator was removed from the stage CFD analysis of the baseline stage with tipshroud. Static pressure profiles at stator exit from the stage analysis were extracted. Standalone rotor with tipshroud was analyzed with stator exit pressure profile. Boundary conditions imposed at inlet were the two static pressure profiles - one from baseline stage analysis and the other from the modified flow path stage analysis. Both the profiles are shown in Fig.20a. With rotor alone analysis done, performance was monitored as isentropic efficiency across rotor alone. Difference in efficiency numbers between the two profiles was around 0.25 % with baseline flow path profile performing better. For the case with baseline pressure profile, the leakage flow was relatively lesser than the case with static pressure profile from modified flow path. This confirms the importance of stator exit static pressure on rotor performance with tip shroud.

Experiments

Motivation

Fig.25 shows a stator and rotor in high pressure section of SST-900 industrial steam turbine. It can be observed that the stator has varying chord along the height of the blade. Discussions and understanding revealed that the variation of chord along blade height was due to ease of manufacturing rather than aerodynamic purpose as the design intent.

With this background, the research objective for the present study is to investigate the differences in aerodynamic behavior between two designs, viz. constant chord along the span and varying chord along the span. The aim is to quantify the total pressure losses, to study the blade-loading patterns and also to investigate the effects on secondary flows. In order to foster to the research objective stated, both experimental and numerical works are planned. The two designs to be compared, viz. constant-chord design and varying-chord design, are manufactured and tested in a linear cascade wind tunnel. The same cascade is also numerically analyzed using commercially available CFD software. Both the experimental and numerical studies are compared and reported.

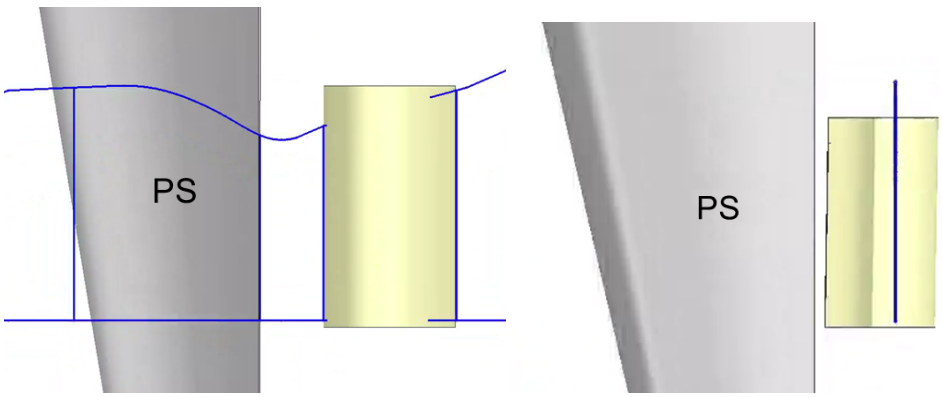

(**a**) Meridional View of HP Stage (**b**) Axial View of HP Stage

Figure 25: High Pressure section stage of SST-900

Methodology and Instrumentation

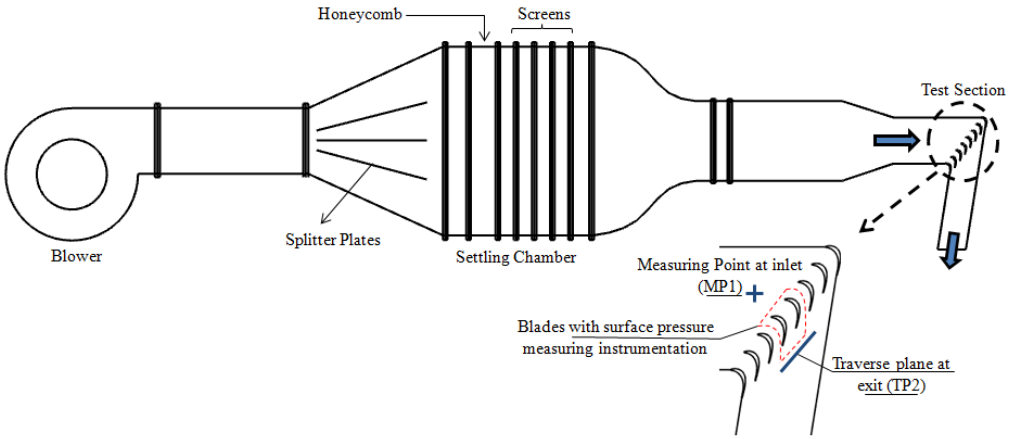

Figure 26: Schematic of the test section.

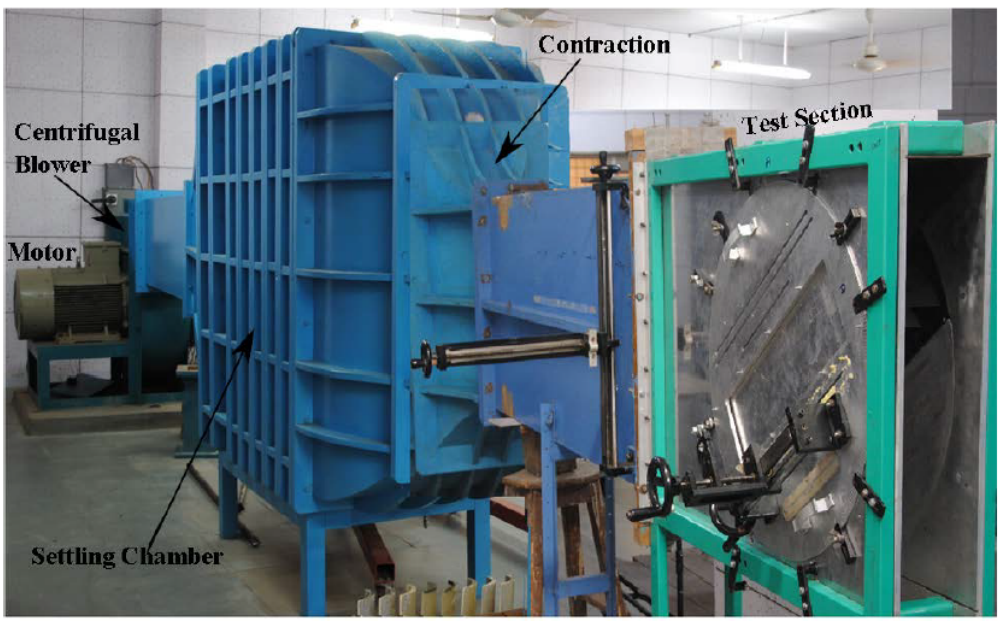

Figure 27: Photograph of the Wind Tunnel.

The experimental investigations were carried out in a low speed, open circuit linear cascade wind tunnel at the Turbomachinery Laboratory, Indian Institute of Technology, Bombay. A schematic representation of the experimental facility is shown in Fig.26. The air entering the blower is filtered by a filtering screen. The exit flow from the blower enters the settling

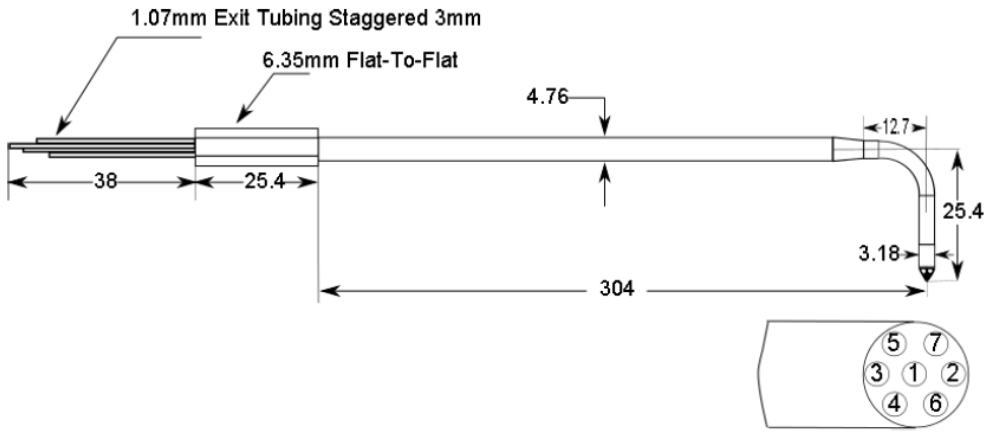

Figure 28: Seven-Hole Probe.

chamber, where it passes through a honeycomb followed by a series of screens. At the exit of the contraction, uniform flow is available, which enters the cascade test section. The test section is a rectangular duct of 398 mm x 150 mm at the entrance of the cascade. The cascade consists of eight blades with the end blades forming the two ends of the test section as shown in Fig.26. At the exit of the blade, the test section follows the camber line path. Fig.27 shows the wind tunnel and test section arrangement in the laboratory.

The inlet flow conditions are measured using manual traverse with pitot tube at approximately one chord length from the leading edge of the cascade (Refer Fig.26). This location is marked as MP1. The stagnation pressure profile required as boundary condition for the numerical analysis is also extracted at this location. An auto-traverse mechanism at the exit of the blade row enables a seven-hole probe (from M/s. Aeroprobe Inc, USA) to be traversed in order to measure the flow conditions. A seven-hole probe is shown in Fig.28. The least count of the traverse mechanism is 1 mm. Also, a traverse of 4 mm with one revolution of the lead screw could be achieved. The 7-hole probe can measure the flow speed over a range of Mach 0.02 to Mach 2. The flow angle of receptivity is $\pm 70°$. The sampling rate of data acquisition is 250 Hz and the sample size is 500. The seven-hole probe is connected to 16 channels Digital Sensor Array (DSA 3217 from M/s. Scanivalve Corp, USA). For a detailed uncertainty analysis of the instruments used, one is encouraged to refer the work by Varpe et al [36]. The traverse plane is approximately one third of the chord length downstream of trailing edge. This traverse plane is shown as TP2 in Fig.26. The matrix to be traversed by the seven-hole probe covers one tangential pitch of the cascade.

The instrumentation necessary for surface pressure measurements on the blade to evaluate the blade-loading is made available on the two blades at the center of the cascade as shown

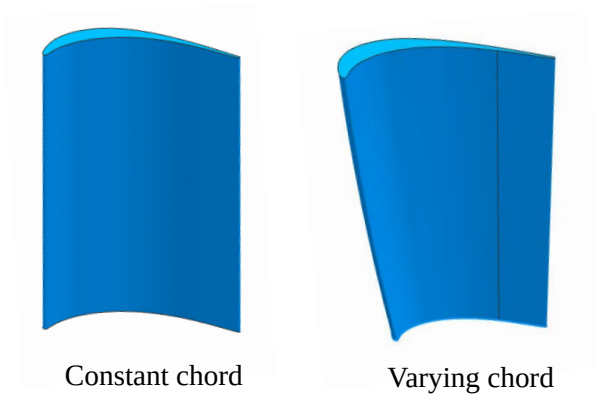

Figure 29: Cascade designs.

in Fig.26. The 0.3 mm static pressure taps on the blade surfaces are connected to the computer through 16 channel digital sensor arrays. The static pressure readings on the pressure surface and the suction surface are captured by two separate sensor arrays.

The cascade blades tested and analyzed in the present work comprise T106 airfoil sections [37]. Two cascade designs are tested: constant-chord design and varying-chord design. The models of the two designs are shown in Fig.29. As the name indicates, the chord of the T106 airfoil section is constant along the blade height in constant-chord design. However, in the varying-chord design, the midspan airfoil section is retained from the constant-chord design. The tip and the root airfoil sections are scaled up and scaled down respectively. The chord lengths at different blade heights for both the designs are compared in Table.3. The cascade details for the constant-chord design are provided in Table.4.

Table 3: Chord details for the two designs

z/h location	Constant chord (mm)	Varying chord (mm)
1	100	114
0.5	100	100
0	100	85

Numerical Methodology

The three-dimensional numerical analysis of a single cascade blade passage is carried out using the commercial software ANSYS® CFX™. The CFD context models are built using a commercial modelling tool. A single cascade blade is modeled using hexahedral mesh.

Table 4: Cascade details

Parameter	Value
Chord [mm]	100
Blade height [mm]	150
Pitch [mm]	71.4
Aspect ratio	1.5
Inlet design angle, degrees	37.7
Exit design angle, degrees	63.2
Reynolds number at exit based on blade chord	3.0×10^5
Number of blades	8

ICEMCFD^{TM} is used for meshing. The mesh size of the cascade is around 2 million, which is based on a grid sensitivity analysis. The boundary layer refinement with a target y^+ on all wall boundaries to be unity is maintained. The magnitude of post analysis numbers for y^+ is less than 1 at all wall boundaries. Steady state RANS simulations are performed. The $k - \omega$ SST turbulence model is used and the convergence criteria is set to 1×10^{-5} for momentum and energy residuals. Furthermore, for all the cases analyzed, mass and energy imbalance is maintained below 0.001 %.The inlet boundary is located at inlet measurement location (MP1). The exit boundary plane is extended beyond the traverse plane location in the experiment by one chord length.

The boundary conditions for the analysis are derived from the experimental data measured. At the inlet, the stagnation pressure profile obtained at MP1 is used. At the exit, an area averaged static pressure value from the experimental data at traverse plane is imposed as the boundary condition. A single cascade blade passage is analyzed assuming a periodic flow.

The periodic flow assumption in the single passage analysis is justified by CFD and experiments. In order to check if the flow is periodic in reality, total pressure readings were taken at traverse location TP2. At mid-span of the blade row, readings were taken for approximately three blade passages. The resulting ratio of P_t to mass averaged P_t is shown in Fig.30a. It can be noticed that the flow is periodic in reality with the constructed test section. A three-dimensional CFD analysis of all the eight blades and the hardware of the test section is performed. The entire test section is modeled with hexahedral mesh. Iso-Mach contours from this CFD run are shown in Fig.30b. The CFD reveals that the number of blades and the hardware are sufficient to generate periodic flow.

Results and Discussion

This section starts with a discussion of the effect of spanwise variation of chord on the blade-loading. Fig.31 shows the comparison in blade-loading for the two designs. Both

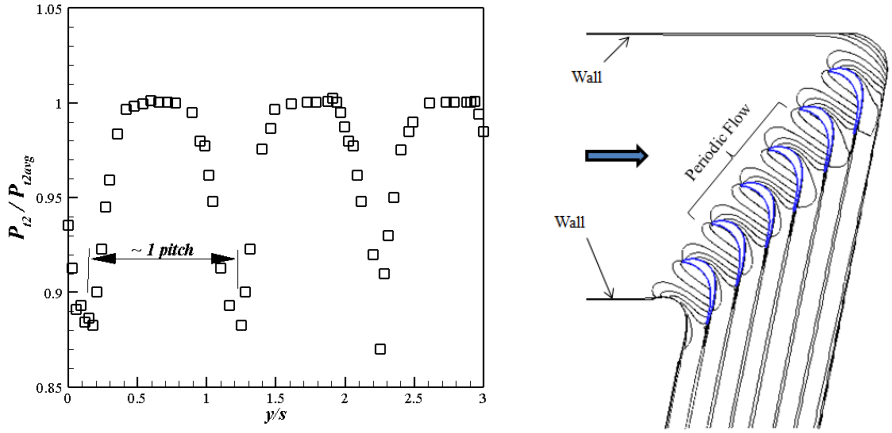

(a) Periodicity from experiment

(b) Periodicity from CFD

Figure 30: Periodicity Check

experimental and CFD results are compared.

Fig.31a shows the blade-loading at *z/h*=0.1 ,where the chord in varying chord design is relatively small when compared to the constant-chord design. It can be observed that due to the decreased chord and the maintained pressure ratio, the blade-loading in the varying-chord design is increased. The gradient of acceleration on the suction side of the airfoil increased in the varying-chord design. The diffusion on the suction side after the peak Mach number is not smooth. The location of peak Mach number on the suction side in the constant-chord design is around 0.7 chord length. However, for the varying-chord design, the peak Mach number on the suction side is around 0.5 chord length.
From the blade-loading plots at *z/h*=0.9 shown in Fig.31b, it can be observed that blade-loading for the increased chord in the varying-chord design decreases. The path of acceleration to the peak Mach number on suction side in the varying-chord design has two distinct gradients. One, mild acceleration till 0.5 chord length. Two, high acceleration from 0.5 to 0.7 chord length where the peak Mach number is reached. Importantly, the area covered by the curves is decreased in the varying-chord design by virtue of the increased chord.
At *z/h*=0.5, since the airfoil sections are the same, the blade-loading values are also the same. This is verified but is not shown here.
The blade-loading plots (refer Fig.31) from the experiment and CFD show similar trends and comparable blade-loading values. This validates the CFD process adopted in the present study. Also, it can be noted that the cascade designs considered expand to the same exit pressure as per design intent. The results shown in this section are as per expected trends. However, since the wetted surface is higher in the zone of increased chord, there is a possibility of increased frictional losses. Since there is a possibility of increased profile loss

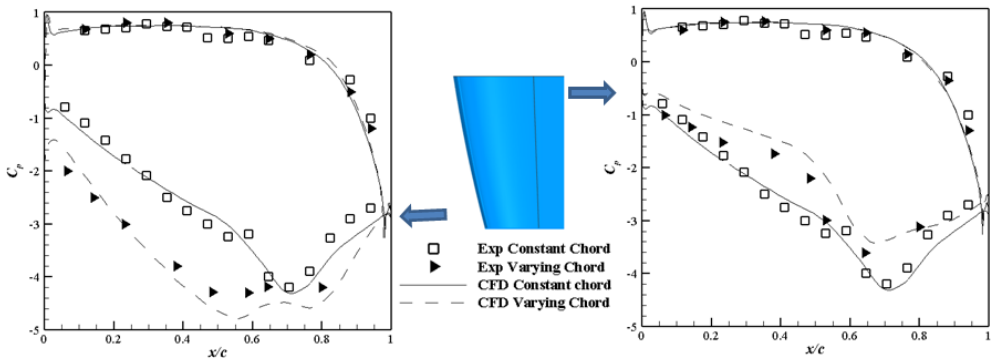

a. Blade loading at $z/h = 0.1$

b. Blade loading at $z/h = 0.9$

Figure 31: Blade loading comparison.

in the region of the increased chord, the effects on profile loss due to varying-chord needs to be studied.

To isolate the effect of design change on profile losses, numerical simulations are used. As described by Yoon et al [38], numerical simulations can be used in order to corner out the loss mechanism that contributes most to the overall losses. However, in the present study, numerical simulations are used to predict a trend in the profile losses.

The numerical simulations are carried out on the cascade domain with free-slip endwalls. As an example, the CFD domain for constant-chord design is shown in Fig.32a. Since the main objective of the CFD analysis with free-slip wall is to compare the trends in profiles losses between the two designs, the inlet total pressure *profile* is not provided as inlet boundary condition. To make the inlet boundary condition void of vorticity, a total pressure *profile* is not given as boundary condition. Instead, mass averaged total pressure value is imposed at the inlet of the domain. At the exit, average static pressure from the experiments is used as the boundary condition.

The total pressure losses from the CFD run with free-slip endwall conditions are shown in Fig.32b. Since there are no secondary losses in the streamwise direction, the total pressure losses can be coined as profile losses. The profile loss values are compared at the traverse location. It can be observed that above z/h=0.5 where the chord increases in the varying-chord design, the profile losses are lower than that in the constant-chord design. On the other hand, the profile losses increases below z/h=0.5 in the varying-chord design where the chord decreases. In the region of z/h=0.5, the profile losses for both the designs are comparable. With the decrease in profile losses with higher chord and increase in profile loss with reduced chord, the overall one-dimensional value of the profile loss in the varying-chord design is similar to the profile loss from the constant-chord design.

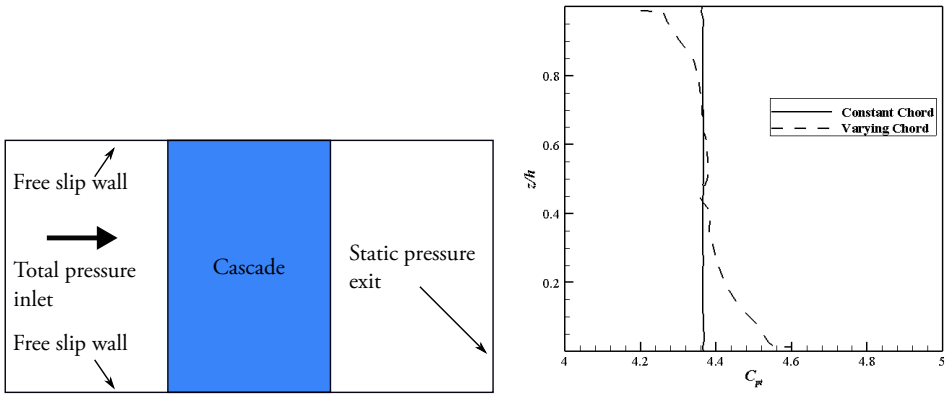

(**a**) CFD domain with free-slip endwall (**b**) Profile loss comparison from CFD

Figure 32: Free slip endwall configuration

Since the CFD predictions are validated in the present study, the trends shown in profile loss predictions can be considered as representing the actual flow scenario. It can therefore be understood that, the scaling of the airfoil section to obtain larger chord length does not increase the frictional losses due to increased wetted surface. Since there is no incident vorticity on the cascade geometry, and hence no source of secondary losses, the loss pattern seen in Fig.32b is relatively smooth towards the endwalls.

In order to study the secondary flow behavior in the constant-chord design and the varying-chord design, coefficient of secondary kinetic energy (CSKE) is used as the objective function. The definition of CSKE used in present study is taken from the work by Corral et al [3]. According to this definition of CSKE a zero value of CSKE corresponds to clean flow or primary flow or flow void of secondary flow. Any value of CSKE other than zero corresponds to deviation from the primary flow and can hence be termed as secondary flow.

Fig.33a shows the CSKE comparison between the two designs from the extracted experimental data at the traverse location. In the mid-blade region (around z/h=0.5), CSKE values are zero, which reveals that the flow is void of streamwise vorticity. Towards the endwall zone where z/h=0, the region affected by secondary flow is almost comparable for the constant-chord design and the varying-chord design. However, in the region above z/h=0.6, the secondary flow patterns between the designs differ. In the varying-chord design, the secondary flow patterns is significantly higher than that in the constant-chord design above z/h=0.6.

Also, Fig.33a indicates that the onset of secondary flow in the constant-chord design is

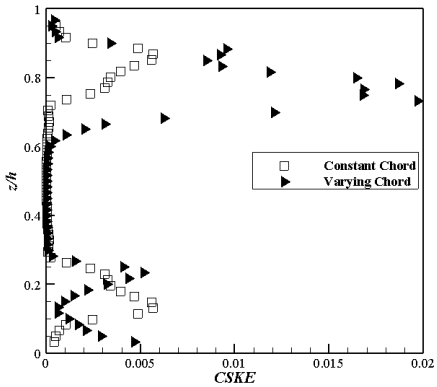

(a) Secondary loss comparison from experiments

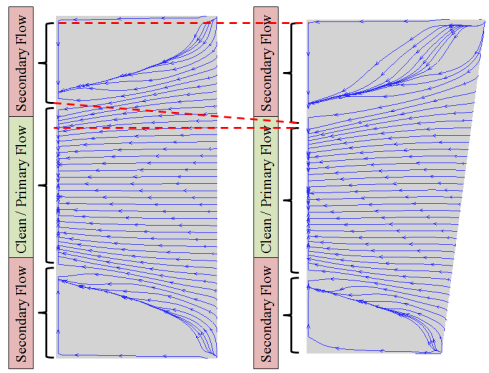

(b) Streamlines on suction surface of cascades (CFD)

Figure 33: Secondary Flow Behavior

around z/h=0.7. In the varying-chord design, flow above z/h=0.6 can be considered to be secondary flow. Hence, the point at which flow deviates from the primary flow is lower in the varying-chord design than in the constant-chord design. This shows that in the region of higher chord, the secondary losses are higher when compared to the constant-chord design for the given conditions.

The trends seen in CSKE plot can be visualized by streamlines extracted from CFD simulations. Fig.33b shows the surface streamlines on suction side of cascade designs. In the figure, approximate regions of primary flow/ clean flow are marked. Also marked are the secondary flow regions. In the varying-chord design, increase in secondary flow region, as seen in CSKE plots from experiments, is indicated. In the region towards z/h=0, the region affected by secondary flow is almost comparable between the designs. From one-dimensional values, the CSKE value in varying-chord design is close to three times of CSKE value in the constant-chord design.

In the varying-chord design, in the region of larger chord, profile loss is relatively low and secondary loss is relatively high when compared to the constant-chord design. It would be interesting to understand the overall loss(C_{pt}) pattern in both the designs.

The variation of C_{pt} along the blade height will be discussed for both the designs. The variation of C_{pt} along blade height is shown in Fig.34a. The values plotted are extracted from the experimental data.
In the zone above z/h=0.6, C_{pt} is higher for the varying-chord design. In this region, it can be observed that the profile losses are relatively low (refer Fig.32b) when compared to the constant-chord design. However, secondary losses are higher from the CSKE assessments. The overall losses being higher in this region suggests that secondary losses are the

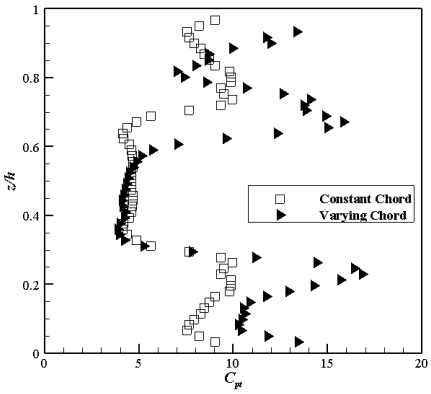

(a) Overall loss comparison from experiments

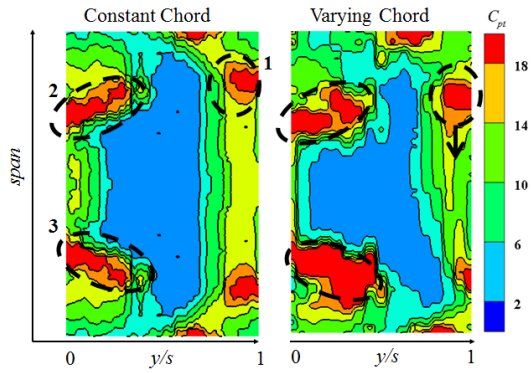

(b) Contour at traverse plane from experiments

Figure 34: Overall Loss Behavior

dominating losses in this zone for the existing setup.

In the zone below z/h=0.3, the overall losses in the varying-chord design is higher. The chord being lower in this region, the profile losses are observed to be higher (refer Fig.32b). From the CSKE evaluation, the secondary losses in the varying-chord design below z/h=0.3 are comparable to the constant-chord design. Since the overall losses being higher with higher profile losses and comparable secondary losses, it can be stated that profile losses are more dominating in this zone. Hence profile losses contribute significantly to the overall pressure losses.

The one-dimensional mass flow averaged C_{pt} values from both experiments and CFD for the designs are shown in Table.5. From the comparison, it can be estimated that C_{pt} is increased by two percentage in varying chord design.

Table 5: Overall loss comparison

	Experiments	CFD
Constant chord	7.08	7.53
Varying chord	9.36	10.12

At the traverse plane, measurements are taken across a matrix to cover one blade passage and a blade height. Contours are generated calculating losses at each point measured. Fig.34b shows the contours of C_{pt} at traverse plane from the measured data. There are three regions marked in the contour for constant-chord with numbers 1, 2 and 3. Considering region 1 in both the designs, it can be observed that there is a shift in region downwards in the

varying-chord design. The same is indicated by a downward arrow in the varying-chord design. This shows there is a hint of flow migration from the higher chord zone to the lower chord zone. The area covered by loss region also increases in varying-chord design in region 1. In region 2 and region 3, the losses are higher in the varying-chord design compared to the constant-chord design.

With the effect of spanwise variation of chord discussed, it is clear that more investigations and enough care needs to be taken from the various loss mechanisms point of view. Profile losses and secondary losses have to be taken into account in the design exercise. From the present study and for the given test section, secondary losses are seen to be the dominating loss mechanism.

Conclusions

In order to increase the efficiency of a turbine stage, the two main loss mechanisms in turbine flows - profile losses and secondary losses were targetted. The redesign of an existing turbine stage in SST-900 industrial steam turbine is attempted. The challenge was to abide by the constraints to maintain the non-dimensional parameters defining the stage. A numerical approach to verify the designed stage was adopted.

With the aim of reducing profile losses, airfoils of stator and rotor were redesigned. The three-dimensional RANS analysis predicts that, through minimizing the incidence losses in rotor, efficiency is improved by 0.17 % for given geometry. Though being prismatic, a better inlet metal angle resulted in significant improvement in total to total stage efficiency. Furthermore, the unwanted loss of overcoming adverse pressure gradient at the leading edge is avoided and hence, advantage is seen.

Improvement in rotor design was further considered to reduce the peak Mach number, as there is hardly any acceleration of flow in the rotor due to low reaction. The gain in total to total efficiency due to this change, predicted by CFD, was 0.06 %. Secondary loss reduction was also spotted by improvement in the rotor airfoil section design. Front loaded airfoil performs better for rotor geometry considered.

The stator was then redesigned with the target of delaying the transition from the laminar to the turbulent boundary layer. The redesigned stator was relatively aft-loaded. Total pressure loss in the redesigned stator reduced by a delta of 0.14, as calculated from CFD analysis. Also, through redesigning the stator, efficiency of stage increased by delta of 0.1 %.

The airfoil design improvement in the stator and the rotor, analyzed numerically, predicted an advantage of 0.33 % in total to total stage efficiency. Further iterations with pitch-to-chord ratio of stator and rotor increased the efficiency further to make an overall improvement of 0.74 %.

Secondary losses were reduced also with SKEH and CSKE monitors showing good advantage with the redesigned stators. However, the total-to-total efficiency numbers did not show the advantage obtained in the stator blade row. The loss behavior in the rotor with the stator modification needs to be studied further in order to understand the exact reason

for numerical methods not revealing the benefits obtained.

Experiments were conducted to check on the aerodynamic performance of the varying chord stator. It was found that prismatic stator performs better aerodynamically. It makes a strong case to make a breakeven analysis for manufacturing costs and aerodynamic gains involved.

References

[1] Uwe HOFFSTADT. Boxberg achieves world record for efficiency. Modern power systems, (OCT):21–23, 2001.

[2] T Germain, M Nagel, and RD Baier. Visualisation and quantification of secondary flows: Application to turbine bladings with 3d-endwalls. In Paper ISAIF8-0098, Proc. of the 8th Int. Symposium on Experimental and Computational Aerothermodynamics of Internal Flows, Lyon, 2007.

[3] Roque Corral and Fernando Gisbert. Profiled end wall design using an adjoint navier–stokes solver. Journal of Turbomachinery, 130(2):021011, 2008.

[4] BR Haller. Vki lecture series on "secondary and tip clearance flows in axial turbines". Full 3D turbine blade design, pages 10–13, 1997.

[5] S Havakechian and R Greim. Aerodynamic design of 50 per cent reaction steam turbines. Proceedings of the Institution of Mechanical Engineers, Part C: Journal of Mechanical Engineering Science, 213(1):1–25, 1999.

[6] J Denton. Loss mechanisms in turbomachines. In ASME 1993 International Gas Turbine and Aeroengine Congress and Exposition, pages V002T14A001–V002T14A001. American Society of Mechanical Engineers, 1993.

[7] John D Coull and Howard P Hodson. Predicting the profile loss of high-lift low pressure turbines. Journal of Turbomachinery, 134(2):021002, 2012.

[8] John D Coull, Richard L Thomas, and Howard P Hodson. Velocity distributions for low pressure turbines. Journal of Turbomachinery, 132(4):041006, 2010.

[9] T Zoric, I Popovic, SA Sjolander, T Praisner, and E Grover. Comparative investigation of three highly loaded lp turbine airfoils: Part i measured profile and secondary losses at design incidence. In ASME Turbo Expo 2007: Power for Land, Sea, and Air, pages 621–630. American Society of Mechanical Engineers, 2007.

[10] Arthur Huang. Loss mechanisms in turbine tip clearance flows. PhD thesis, Massachusetts Institute of Technology, 2011.

[11] SM Goobie, SH Moustapha, and SA Sjolander. An experimental investigation of the effect of incidence on the two-dimensional performance of an axial turbine cascade. In Proceedings, Ninth International Symposium on Air Breathing Engines, volume 1, pages 197–204, 1989.

[12] Teik Lin Chu. Effects of mach number and flow incidence on aerodynamic losses of steam turbine blades. 1999.

[13] MW Benner, SA Sjolander, and SH Moustapha. Influence of leading-edge geometry on profile losses in turbines at off-design incidence: experimental results and an improved correlation. Journal of turbomachinery, 119(2):193–200, 1997.

[14] SH Moustapha, SC Kacker, and B Tremblay. An improved incidence losses prediction method for turbine airfoils. Journal of Turbomachinery, 112(2):267–276, 1990.

[15] Theodosios Korakianitis and Paschalis Papagiannidis. Surface-curvature-distribution effects on turbine-cascade performance. In ASME 1992 International Gas Turbine and Aeroengine Congress and Exposition, pages V001T01A044–V001T01A044. American Society of Mechanical Engineers, 1992.

[16] Theodosios Korakianitis. Prescribed-curvature-distribution airfoils for the preliminary geometric design of axial-turbomachinery cascades. Journal of turbomachinery, 115(2):325–333, 1993.

[17] DG Ainley and GCR Mathieson. A method of performance estimation for axial-flow turbines. Citeseer, 1951.

[18] AG Klebanov and BI Mamaev. Optimal pitch for a turbine blade cascade. Thermal Engineering, 16(10):79, 1969.

[19] O Zweifel. The spacing of turbo-machine blading, especially with large angular deflection. Brown Boveri Rev., 32(12):436–444, 1945.

[20] W Traupel. Thermische turbomaschinen (thermal turbo-machinery), first vol, 1977.

[21] S. C. Kacker and U. Okapuu. A mean line prediction method for axial flow turbine efficiency. Journal of Engineering for Power, 104:111, January 1982.

[22] Aurel Stodola. Dampf-und Gasturbinen: mit einem Anhang über die Aussichten der Wärmekraftmaschinen. J. Springer, 1922.

[23] David Japikse, Nicholas Baines, et al. Introduction to turbomachinery. 1994.

[24] E Dejc, GA Filipov, and L Ya Lazarev. Atlas of axial turbine blade characteristics, 1965.

[25] JD Denton and L Xu. The exploitation of three-dimensional flow in turbomachinery design. Proceedings of the Institution of Mechanical Engineers, Part C: Journal of Mechanical Engineering Science, 213(2):125–137, 1998.

[26] Peter John Walker. Blade lean in axial turbines: model turbine measurements and simulation by a novel numerical method. PhD thesis, University of Cambridge, 1987.

[27] H Kawagishi and S Kawasaki. The effect of nozzle lean on turbine efficiency. ASME Paper, (H00652), 1991.

[28] A Nowi and BR Haller. Developments in steam turbine efficiency. VGB KRAFT-WERKSTECHNIK-ENGLISH EDITION-, 77:499–503, 1997.

[29] Budimir Rosic and Liping Xu. Blade lean and shroud leakage flows in low aspect ratio turbines. Journal of Turbomachinery, 134(3):031003, 2012.

[30] ME Deich, AE Zaryankin, GA Fillipov, and MF Zatsepin. Method of increasing the efficiency of turbine stages with short blades. Teploenergetika, 2:240–254, 1960.

[31] MJ Atkins. Secondary losses and end-wall profiling in a turbine cascade. IMechE Paper C255, 87, 1987.

[32] AWH Morris and RG Hoare. Secondary loss measurements in a cascade of turbine blades with meridional wall profiling. In American Society of Mechanical Engineers, Winter Annual Meeting, Houston, Tex, page 1975, 1975.

[33] John I Cofer. Advances in steam path technology. Journal of engineering for gas turbines and power, 118(2):337–352, 1996.

[34] Arno Duden, Irene Raab, and Leonhard Fottner. Controlling the secondary flow in a turbine cascade by 3d airfoil design and endwall contouring. In ASME 1998 International Gas Turbine and Aeroengine Congress and Exhibition, pages V001T01A023–V001T01A023. American Society of Mechanical Engineers, 1998.

[35] MF El-Dosoky, Aldo Rona, and Jonathan Paul Gostelow. An analytical model for over-shroud leakage losses in a shrouded turbine stage. In ASME Turbo Expo 2007: Power for Land, Sea, and Air, pages 773–782. American Society of Mechanical Engineers, 2007.

[36] Mahesh K. Varpe. Endwall contouring in a low speed axial flow compressor cascade. PhD thesis, Indian Institute of Technology, Bombay, 2015.

[37] Rory Douglas Stieger. The effect of wakes on separating boundary layers in low pressure turbines. PhD thesis, University of Cambridge, 2002.

[38] Sungho Yoon, Thomas Vandeputte, Hiteshkumar Mistry, Jonathan Ong, and Alexander Stein. Loss audit of a turbine stage. Journal of Turbomachinery, 138(5):051004, January 2016.

Scientific publications

Author contributions

Paper I: Efficiency Improvements In An Industrial Steam Turbine Stage - Part 1

My contributions : Designed and numerically verified front-loaded and aft-loaded airfoil designs for rotor and stator. Addressed the incidence issues in the rotor design and significant efficiency improvement was achieved. Rotor and stator airfoils were redesigned while complying to the design constraints.
MG, MT : Supervised the work carried out.

Paper II: Vortexing Methods to Reduce Secondary Losses in a Low Reaction Industrial Turbine

My contributions : Designed and analyzed three vortexing methodologies on the stator - Free vortex, Inverse Vortex and Parabolic Forced Vortex. The design intent was to reduce the secondary losses using Vortexing. CFD analysis reveals that the secondary losses are reduced in inverse vortex and parabolic forced vortex designs.
MG, MT : Supervised the work carried out.

Paper III: Influence of Compound Lean on an Industrial Steam Turbine Stage

My contributions : Three dimensional design of stator where in pressure side leaning towards the end walls was attempted. Compound lean stators with two lean angles were designed. Primarily, leaning was attempted to reduce the secondary losses. From the CFD analysis, secondary losses were lesser in compound lean cases.
MG, MT : Supervised the work carried out.

Paper IV: Reduction in Secondary Losses in Turbine Cascade Using Contoured Boundary Layer Fence

My contributions : Based on the hypotheses of breaking the vortex lines to reduce vortex strength and accelerating the flow by reducing flow area, T106 cascade was modified to

accomodate boundary layer fence. Secondary losses were significantly reduced. Helicity was used to quantify and monitor the secondary losses.
MG, MT : Supervised the work carried out.

Paper v: Efficiency Improvements In An Industrial Steam Turbine Stage - Part 2

My contributions : Flow path modifications were considered in this paper. Axisymmetric endwall contouring present in the baseline flow path was evaluated. It was found that the endwall contouring helps to reduce the tip leakage flows and hence contributes to the efficiency gain. Elaborate leakage flow modelling was performed.
MG, MT : Supervised the work carried out.

Paper vi: Effect Of Spanwise Variation of Chord On The Performance Of A Turbine Cascade

My contributions : Spanwise variation of chord exists in the high pressure section of the steam turbine considered. This was discussed to be present for manufacturing reasons. Experiments and numerical studies were initiated in order to check the aerodynamic flow behavior of two cascade designs - constant spanwise chord and varying spanwise chord. The two designs were looked at from perspective of different loss mechanism that affect the performance like profiles losses, secondary losses and overall losses.
AMP, MG, MT : Supervised the work carried out.